The Role of Corals on Tsunami Dynamics in an Island Setting: A Case Study of

Tutuila Island

Derya Itir Dilmen

A dissertation

submitted in partial fulfillment of the

requirements for the degree of

Doctor of Philosophy

University of Washington

2016

Reading Committee:

Vasily V. Titov, Chair

Gerard H. Roe

Joanne Bourgeois

Program Authorized to Offer Degree:

Earth and Space Sciences

University of Washington

Abstract

The Role of Coral Reefs on Tsunami Dynamics in an Island Setting: A Case Study of Tutuila

Island

Derya Itir Dilmen

Chair of the Supervisory Committee:
Affiliate Professor Vasily V. Titov
Earth and Space Sciences

On September 29, 2009 at 17:48 UTC, an Mw = 8.1 earthquake in the Tonga Trench generated a tsunami that caused heavy damage across Samoa, American Samoa, and Tonga. One of the worst localities hit was the volcanic island of Tutuila in American Samoa. Tutuila Island, located 250 km from earthquake epicenter, experienced tsunami inundation and strong currents on the north and east coasts, causing 34 fatalities and widespread structural and ecological damage. The surrounding coral reefs of the island also suffered heavy damage. This damage was formally evaluated based on detailed surveys before and immediately after the tsunami, which provides a unique opportunity to evaluate the role of coral reefs on tsunami dynamics.

In the first part of this research, estimates of tsunami dynamics are obtained with the MOST numerical tsunami model (Titov and Synolakis, 1997), which is currently the operational tsunami forecast tool used by the US National Oceanic and Atmospheric Administration (NOAA). The earthquake source function was constrained using real-time deep-ocean tsunami data from three DART® (Deep-ocean Assessment and Reporting for Tsunamis) systems in the far field, and by tide-gauge observations in the near field. We compare the numerically estimated run-up with observations to evaluate the simulation skill of MOST. We present an overall synthesis of tide-gage data, survey results of the run up, inundation measurements, and the datasets of coral damage around the island, in order to evaluate the overall accuracy of MOST run-up prediction for Tutuila and the model's performance of simulating in the locations covered with corals during the tsunami event. Our primary findings are 1) there is a tendency for MOST to underestimate run-up on Tutuila and 2) the locations where the model underestimates run-up tend to have experienced heavy or very heavy coral damage, whereas well-estimated run-up locations characteristically experienced low or very low damage. This brought us to the conclusion regarding how coral reefs affect tsunami dynamics through their influence on bathymetry and dissipation.

Second, we focus on numerical simulations of this event to evaluate: 1) how roughness variations affect tsunami run-up and if different values of Manning's roughness, n, improve the simulated run-up compared to observations; and 2) how depth variations in coral reef bathymetry control run-up and inundation on the coastlines they shield. We find as a result of the simulations that no single value of n provides the best match to observations, and we find large bay-to-bay variations in the impact of varying n. The results suggest that there are aspects of tsunami wave dissipation that are not captured by the drag formulation in the MOST model. The

primary impact of removing coral bathymetry is to reduce run-up, from which we conclude that at least in this setting the bathymetric impact of coral reefs is to increase run-up and inundation. We conclude that future studies should focus on two key issues for further research: 1) the representation of the turbulent dissipation in terms of the governing equations and their coefficients and 2) detailed numerical experiments on all aspects of reef settings such as reef widths, reef types and coastal geometry on the scale of individual bays.

TABLE OF CONTENTS

LIST OF FIGURES

LIST OF TABLES

ACKNOWLEDGEMENTS

DEDICATION

to my mom

Chapter 1. INTRODUCTION

1.1   THE PHENOMENON OF TSUNAMIS

Tsunamis are among the deadliest natural hazards on Earth. They have caused over 400,000 fatalities in the last century, ranking them fourth after earthquakes, floods, and volcanic eruptions (NGDC/NOAA, 2015). The threats we face from tsunamis are 1) direct deaths and injuries, 2) structural and ecological damage and 3) the subsequent spread of diseases and harmful chemical substances.

A tsunami is a long series of low-crested gravity waves, often generated by the energy transferred from a seafloor displacement to the ocean. The global historical tsunami database of the (National Geophysical Data Center[1] / World Data Source NGDC/WDS) provides information on over 2,400 tsunamis from 2100 BC to the present in the Pacific, Atlantic, and Indian oceans; and the Mediterranean and Caribbean seas (NGDC/WDS, 2015) of which 75% of those recorded tsunamis occurred due to earthquakes. Most large tsunamis are caused by the seafloor displacement due to large shallow earthquakes along subduction zones. Less commonly, non-subduction-zone earthquakes, landslides, volcanic eruptions, nuclear explosions, meteorite impacts, and meteorological events also generate tsunamis (Gusiakov, 2007).

Etymologically the term "*tsunami*" comes from Japanese, *"tsu"- breaking upon a harbour; "name"-waves*. These phenomena were called harbor waves because of strong water currents, unexpected wave oscillations, and damage to harbors were the first signs of an approaching tsunami for far-field events.

---

[1] NOAA's National Geophysical Data Center, NGDC, was recently renamed the National Centers for Environmental Information, NCEI; the website remains https://www.ngdc.noaa.gov/ as of August 2016. In this dissertation I refer to the tsunami database source by its more familiar name, NGDC

An early appearance of the word "tsunami" in western literature was an article by Eliza Schidmore in *National Geographic* about the 1896 Sanriku tsunami, which killed more than 22,000 people (Cartwright & Nakamura, 2008; Schidmore, 1896). Although always in the minds of shore-dwelling populations in high-risk areas, tsunami hazards received a renewed public focus on tsunami hazards came after the devastating Indian Ocean Tsunami of 26 December 2004, which took close to 230,000 lives and injured countless more (USGS, 2005). Further sobering evidence of the power of tsunamis to wreak destruction was the Great Japan earthquake and tsunami of 11 March 2011, which - even in this tsunami-aware and prepared society - claimed nearly 16,000 lives, Subsequently, tsunami generated flooding caused a nuclear meltdown and radiation leaks at Fukushima, which led to the permanent dislocation of a 230,000 people (Oskin, 2015).

1.2 THE GENERATION OF TSUNAMIS

A typical tsunami begins with a rupture on a submarine plate-boundary fault, which displaces the ocean floor and transmits a dynamic impulse to the water column. Gravity acts to restore mean sea level by converting the potential energy of the water displacement into gravity waves. These waves radiate the resulting potential energy away from the source of the tsunami and propagate through the ocean till they reach shorelines.

The size of the tsunami depends on the main parameters that govern the earthquake: the energy release (magnitude); the source mechanism and depth of the hypocenter; the fault rupture velocity; and water depth over the source region. Earthquakes with large magnitudes (greater than 8 in Moment Magnitude Scale), and shallow hypocenters (< 30 km depth in Earth) produce the largest tsunamis.

1.2.1 *The Three Stages of the Tsunami*

There are three major stages associated with a tsunami: generation, propagation, and run-up/inundation:

During a typical tsunamigenic submarine earthquake, a segment of ocean floor is rapidly uplifted and displaces a volume of water; some other part of the seafloor may also subside. This creates a hump or trough on the ocean surface, which is unstable due to the force of gravity. The pressure gradient formed due to gravity causes waves to flow sideways, generating a train of waves, a tsunami. Okada (1985) derived the equation for the initial displacement of the ocean surface by computing the static field of vertical deformation on the ocean floor, assuming the water is incompressible and the deformation occurs in seconds. The model has been widely used in numerical tsunami models to estimate initial tsunami wave amplitudes.

Once generated, tsunami waves can reach coastal areas after traveling hours to days with negligible frictional dissipation in the open ocean (Titov, 1997). However, the wave structure evolves substantially as waves spread out over the bathymetry. When an individual tsunami wave approaches a shoreline it transfers some of its kinetic energy into potential energy. The waves increase in height. The amplified tsunami wave then overruns and inundates the coastline. A broad spectrum of wavelengths formed during tsunami generation leads to dispersion of the wave packet during their travel from the source to the coast; consequently, there can be a prolonged period of repeated shoreline inundation upon the tsunami's arrival at a coastline.

A typical tsunami wave length (10 km to 200 km) is much larger than typical water depths (2-4km) in the deep ocean. Therefore, the propagation of a tsunami can be described accurately by the equations for waves in inviscid shallow-water until the waves approach the shore. These equations are derived from depth-integrated Navier-Stokes equations for conservation of mass

and linear momentum in a fluid. The assumptions of shallow water equations are: the fluid is incompressible (constant density); the horizontal length scale is much greater than the vertical length scale; and the flow is homogeneous (Bricker, et al., 2015).

The shallow-water equations describe a thin layer of fluid, where water depth (h) to wave length (L) ratio is in the order of 10^{-2}. They are subjected to a constant gravitational force, bounded by the bottom topography below, and by a free surface above. In the case of tsunami for shallow-water approximation, the waves are assumed to be non-dispersive and to travel with a linear wave speed *(c)* of:

$$c = \sqrt{gh} \qquad (1.1)$$

where g is gravity and h is the water depth. For deep-ocean conditions where the ocean depth is several kilometers, a tsunami wave velocity of around 200 m/s is typical. Even communities that receive warning may have only minutes or up to a few hours to prepare for trans-oceanic tsunamis to prepare. Within a few minutes after generation, the tsunami develops into a sequence of long wavelength (10 km to 200 km typical depending on source parameters) waves that grow rapidly in height as the tsunami approaches the shore. As the waves approach, the depth of water decreases, causing the tsunami to slow down, at a rate proportional to the square root of the water depth (Eqn. 1.1). Wave shoaling then forces the wave amplitude A to increase at an inverse rate with local undisturbed water depth, h, governed by *Green's law* (Green, 1837), (Eqn. 1.2):

$$A \propto \frac{1}{h^{1/4}} \qquad (1.2)$$

For energetic events, the wave height above sea level at the maximum point of inundation, or 'run-up' can reach upwards of 40 m as seen in 2011 Great Tohoku Japan Tsunami run-up observations (Mori et al., 2011).

When a tsunami finally reaches the shore, it may appear as a rising or falling wave, a series of breaking waves, or a bore. The waves return at intervals of several minutes for up to days before finally dissipating. The geomorphology of the littoral setting strongly affects the tsunami. Submerged features (such as reefs), bays, entrances to rivers, and the slope of the beach all act to modify the dynamics of the tsunami as it approaches the shore, and these numerous influences make it harder to comprehend and model tsunami wave dynamics on the coast. Therefore, understanding the inundation/run-up stage of tsunami is the main objective of tsunami hazard mitigation.

1.3   THE HISTORY OF TSUNAMIS

The present version of the National Geophysical Data Center catalog on tsunamis and tsunami-like events covers the period from 2000 BC till present (NGDC/WDS, 2015). The catalog provides insights into tsunami processes of generation, propagation and inundation run-up. It also helps determine the source of each tsunami with probabilistic and deterministic approaches, identify locations that are particularly prone to tsunamis, and forecast probable inundation limits by combining the data of tsunami source of the NGDC data with probabilistic analyses or computational models. The forecasting results are also crucial to determine wave amplitude thresholds of operational tsunami warnings, and thus whether a tsunami warning will be issued.

According to the NGDC, 2008 catalog, more than 600,000 people have died due to 2130 individual tsunamigenic events since 2000 BC (Whitmore, 2009). Ten trans-oceanic tsunamis during the last 250 years are responsible for 49% of those deaths (Gusiakov, 2007). Of the total 2130 events, 1206 occurred in the Pacific Ocean. Every tsunami is unique, but here I note a few

that have had groundbreaking impact on progress in tsunami research, based primarily on more extensive review by Okal (2011):

The *1755 Lisbon tsunami* remains the deadliest trans-oceanic tsunami in historical times with a death toll approaching 100,000 in Europe (NGDC/WDS, 2015). The effect of this earthquake and tsunami was not only scientific but also was social and political. Since all the churches in Lisbon were destroyed, on All Saints Day, it has been seen as a manifestation of divine judgment (Paice, 2008). Numerical model case studies of this event have been used to demonstrate that even a minor change in fault source location could significantly affect directionality and focusing, resulting in a distinctly different distribution of tsunami wave amplitudes (Zahibo, et al., 2011).

The *1896 Meiji Tsunami,* the first identified "tsunami earthquake" (earthquake whose magnitude is smaller than the magnitude of tsunami created; (Kanamori, 1972), remains the deadliest tsunami in Japan's recorded history. The tsunami was much larger than expected from the amplitude of its seismic waves, with run-up reaching more than 30 m in the near field, up to 5 m in Hawaii, and damage reported in California (Okal et al., 2009).

After the *1933 Great Sanriku tsunami,* buildings were relocated to higher grounds as a first countermeasure against a tsunami (Murao, 2014).

The *1923 Kamchatka tsunami* is considered as the first tsunami for which a far-field warning was given, even though local authorities of Hawaii did not take it seriously. It is an early instance of an insufficient interaction between scientists and decision makers (Okal, 2011).

The *1946 Aleutian Islands tsunami,* is the first tsunami disaster in US history causing fatalities. The tsunami warning center at Honolulu Geomagnetic Observatory was established after this event, in 1949 (Igarashi et al., 2011).

The *1960 Chile tsunami,* was generated by the largest earthquake in the historical record, Mw 9.5, an estimated moment magnitude of 2-5 x 10^{30} dyn.cm. An important lesson learned from this disaster was that the maximum wave during a distant tsunami is rarely the first one. The long periods of tsunami waves can give a sense of feeling secure to residents and to authorities even though the worst is yet to come (Okal, 2011).

The *1964 Alaska tsunami* led the creation of the Alaska/West Coast Tsunami Warning Center in 1967 (Sokolowski, 1990). It was incidentally recorded on a pressure sensor deployed on the ocean floor about 1000 km far from the earthquake epicenter, and which had been installed for an unrelated seafloor magneto-telluric experiment (Filloux, 1982). This observation led to the development of specifically engineered tsunami pressure detectors coupled with real-time communications, creating the Deep Ocean Assessment and Reporting of Tsunami (DART) Network in 2003 by NOAA for the purpose of forecasting coastal tsunami impacts (Bernard & Milburn, 1985).

The *1992 Nicaragua tsunami:* was the first to be systematically surveyed by international teams (Synolakis and Okal, 2005). Such comprehensive and consistent databases of inundation and run-up continue to be used to test tsunami computational model results. This tsunami survey documented substantial values of run-up (4-10 m) along a 290 km stretch of coastline (Satake et al., 1993), which was underestimated by then-standard simulation algorithms that stopped the wave height and current estimations at an imaginary reflective boundary wall, at a shallow-water depth of typically 10 m (Imamura, et al. 1993). In the models, tsunami waves were as much as one order of magnitude smaller than the surveyed values. This led to the introduction of new numerical algorithms for computing run-up and inundation that were able to successfully reproduce the surveyed values of waves penetrating over initially dry land (Titov and Synolakis,

1998). The MOST tsunami code used in this thesis is one of the models developed after this event, and this new suite of models have been tested by laboratory and field survey data for different events and scenarios since then.

For the first time, in 1995, during the *Colima-Jalisco tsunami* in Mexico, the withdrawal of the sea in, was documented with photographs along the southern end of Tenacatita Beach (Borerro, et al., 1995).

The *1998 Papua New Guinea tsunami:* The event has been the subject numerous discussions and controversies due to its unexpected tsunami magnitude and unresolved mechanism of the earthquake. A moderate magnitude of earthquake triggered a submarine landslide, which was the source of a locally catastrophic tsunami, raising awareness of this mode of tsunami generation (Tappin, et al., 2008).

Education on tsunami risk lessened the loss of lives was the lesson taken from this tsunami *1999,* the *Vanuatu tsunami* (Okal, 2011). A few months previously, the 1998 Papua New Guinea tsunami at Vanuatu had occurred and subsequently villagers at Vanuatu were educated to immediately self-evacuate low-lying areas upon feeling strong earthquake tremors, especially if followed by a retreating of sea. In 1999, an earthquake struck the Vanuatu Island and the earthquake-triggered tsunami completely destroyed the village. However, only three residents lost their lives (Caminade, et al., 2000).

The *2003 Aleutian islands tsunami:* This was the first successful operational use of DART buoys in real time (Lautenbacher, 2005).

The *Sumatra-Andaman, 2004 tsunami:* The deadliest tsunami in recorded history with a death toll close to 275,950 was recorded by USGS, 2005. Among its many aspects, the following changed the attitude of researchers, planners and policy makers on both the technical and

operational ways of tsunami risk mitigation (Okal, 2011) (1) communication during the disaster was a failure; (2) tsunamis have come to be regarded as a global threat; (3) caused an acceleration of a global effort to establish tsunami warning centers; (4) funding and research investments from national governments increased to enhance tsunami programs.

2011 Great Tohoku Japan tsunami: Lessons from this event: (1) Safer, more flood resilient buildings - particularly power plants and evacuation structures - are needed. (2) Developing a robust tsunami numerical model for prediction of tsunami impacts is urgent.

1.4 TSUNAMI MODELING AS A TOOL TO PREVENT/DECREASE THE DAMAGE AND LOSS OF LIVES DUE TO TSUNAMIS

After the Great Tohoku Japan tsunami event in 2011, the urgency of developing a robust tsunami numerical model for prediction of tsunami impacts has become obvious and globally accepted. As noted in 2003 by Titov et al. (2003a) "A robust tsunami numerical model should provide site- and event-specific maximum wave amplitude information, well before the first wave arrives at a threatened community and accurate enough to mitigate tsunami hazard in real time". Tools such as, direct tsunami measurements, as well as post tsunami surveys and geological records of tsunami deposits are used to constrain tsunami sources and dynamics in numerical models.

Direct tsunami measurements in the aftermath of a tsunami, taken with tide gauges, and DART - type gauges can assist in validating and analyzing earthquake source characteristics and can be incorporated into numerical tsunami simulations. Starting from 1908, analog tide gauges were used to estimate tsunami wave heights in Japan (Mofjeld, 2009). In the 1960s, tide gauges reported wave height information to warning centers, and were used to determine whether to issue a tsunami warning or just a tsunami watch. Nowadays, they work as calibration and comparison tools for the numerical tsunami models. However, it has been established in

numerous studies (eg. Miller, 1972; Rabinovich, 1997) that the effects of local resonance within the bays or harbors where tide gauges are located have an observable impact on wave characteristics at the tide gauge, limiting their value for predicting run-up (Titov, 2009). Furthermore, the wave period recorded by the tide gauge mostly depends its location rather than on the tsunami source characteristics. On the other hand, bottom-pressure stations (DARTs) installed in the open ocean obtain more direct tsunami wave data before tsunamis develop complex dynamics on the continental shelf and the coastal region, as well as resonance effects inside bays and harbors.

Measuring fluctuations in bottom pressure by transferring the data via satellite to shore, the latest development DART systems provide open-ocean, accurate time series of tsunami water levels for tsunami source analysis (Titov, 2009). The first wave in an observed tsunami time series is particularly important in any analysis related to the tsunami source. This is because it is the least affected by the reflections, scattering, and wave interference that complicate later waves. The timing, amplitude, period and sign (trough or crest wave) of this first wave indicate the pattern of vertical ground displacement of the earthquake source. Numerical models use the first tsunami waves observed at DART Stations to refine the preliminary tsunami sources by inverting the data back to the source using pre-computed model simulations.

Post tsunami surveys including the information of the extent of the tsunami inundation, maximum wave heights on the coast, number of damaging waves, transport of debris, sediment, rock and corals provide a ground truth for remotely sensed data and test cases for numerical models of tsunami inundation. Later post tsunami surveys such as damages in corals help fill the gaps in the measurements. The refined numerical model results by direct tsunami measurements and post tsunami surveys are shared with tsunami warning centers and their related systems to

reduce loss of lives by providing warnings to coastal residents (Whitmore, 2013). Geological records of tsunami deposits also provide test cases, for the inundation modules of the tsunami models (Bourgeois, 2009).

1.5   WHAT ARE THE CHALLENGES TO TSUNAMI MODELING?

In general, the run-up of a tsunami on land will be influenced by a very large number of factors, including the earthquake source (seismic moment and geometry) and its physical environment (earthquake depth, bathymetry of the source area), and the properties of the receiving shoreline (above and below sea level topography of the beach, presence of bays, harbors, estuaries etc.). Other factors can play a role too. All large earthquakes can trigger landslide failures, which in turn can generate tsunamis with run-up values locally much larger than those of the main earthquake. (as in Plafker, 1997).

While the basic equations for numerical analysis of tsunamis have been known for decades, development of numerical models for real-time forecasting has taken over 20 years beginning with the 1993 tsunami modeling efforts of Japan. Models advanced with benchmarks and validation tools such as the large-scale laboratory experiments, analytical methods and DART gauge recordings. The models have evolved through a meticulous process (Synolakis & Kanoglu, 2009) of validation and verification. In a series of workshops on long-wave run-up models in the 1990s, a number of benchmark tests were suggested, comparing numerical solutions to analytical predictions and to certain laboratory measurements (Liu, Woo, & Cho, 1998). The detailed history and background of the benchmarks and tests are summarized in Synolakis, et al., (2008) and in Synolakis and Kanoglu, (2009).

Tsunami models have been developed with a variety of different numerical methods, and of spatial and temporal discretization techniques. The vast majority of current tsunami models are

based either on the Boussinesq or the non-dispersive shallow water (long wave) equations derived from depth-integrated Navier-Stokes equations. In these models, the Navier-Stokes equations are averaged from the seafloor to the free surface, and viscous stresses are either neglected, or presumed to follow bottom friction laws. Depth-averaged Navier-Stokes equations are known as the nonlinear shallow water equations; linearizing the nonlinear terms then gives the linear shallow water equations. Depth-averaged models that study propagation of tsunami waves in one direction are referred to as 1+1, and similarly 2+1 models refer to two-directional propagation. On the coast, wetting-drying algorithms of the models predict tsunami run-up and inundation limits.

When the first advances in numerical tsunami models began in the 1970s in Japan, they were concentrated on solving either non-linear 1+1 Boussinesq equations (reviewed in Shuto and Fujima, 2009) or 2+1 shallow water equations (Synolakis and Kanoglu, 2009). In 1974, Houston and Garcia, (1974) solved a linear form of the spherical long-wave equations in 2+1 form up to the edge of the continental shelf, using a finite difference method. The same year, Hibberd and Peregrine (1974) calculated the evolution of bores over a sloping beach with a shoreline algorithm of non-linear shallow water equations.

Advances in modeling in the 1990s were stimulated through two landmark scientific meetings: the first one was in Russia in 1989, the other was in California in 1990 (Synolakis and Kanoglu, 2009). In 1997, Goto and Ogawa proposed a finite-difference method with upwind scheme in Eulerian form of the non-linear shallow water equations. During the same time interval, at a meeting in Russia, Titov and Synolakis, (1995) presented the finite difference 2+1 algorithm of VTCS, now called MOST, which computes far-field tsunami propagation and inundation in a variable spatial grid for weakly dispersive tsunamis. MOST has been used

operationally by NOAA, and also is the model used in this thesis for tsunami run-up and inundation calculations in Tutuila.

At the 1990 meeting in California, the pervasive need for laboratory data to enable further progress in computational models, particularly for 2+1 run-up computations, found voice.

The following is a review of tsunami models developed by different research groups:
In the early 1990s, Prof. Imamura of the Disaster Center of Japan has developed the TUNAMI (Tohoku University's numerical analysis model for inundation) model, which estimates tsunami propagation in deep water and inundation on land (Imamura, 1996). Currently, TUNAMI has been accepted by 43 organizations in 22 countries as the numerical code to predict damage of tsunami on coasts. It is an open source, fully tested model, evaluated for most of the historical tsunamis such as 1883 Krakatau Tsunami, 1935 North Sumatera Tsunami, 1992 Flores Tsunami, 1994 East Java Tsunami, 1996 Toli-Toli Tsunami, 1996 Biak Tsunami, 2000 Bangai Tsunami, 2004 Aceh Tsunami, and 2006 South Java Tsunami and 2011 Great East Japan Tsunami and benchmark problems (Yalciner, et al., 2014).

Another numerical model, extensively used for tsunami modeling is COMCOT (Cornell Multi-grid Coupled Tsunami model) (Liu, Woo, & Cho, 1998), which is composed of a nested grid system. The system dynamically couples up to 12 levels with different grid resolutions to fulfill the need for tsunami simulations at different scales. In both TUNAMI and COMCOT models, shallow-water equations are used and a flux-conserving algorithm preserves the water mass throughout the computations. COMCOT adopts an explicit staggered, leap-frog, finite difference scheme to solve shallow-water equations in both Spherical and Cartesian coordinates.

In 2001, the Environmental Assessment and Monitoring Department in France developed CEA/DASE. The model is certified and fully tested with benchmark tools. The code has been

also applied for the probable tsunami scenarios in French Polynesia, Pacific and Indian oceans and Mediterranean Sea (eg., Hebert, et al., 2001).

A similar model to CEA/DASE, UBO-TSUFD, was developed by Bologna University, Italy in 2003. The non-linear shallow water equations were solved using finite-element and two-step time integration methods. The grid type is either triangular elements or a Cartesian coordinate system on a fixed boundary. The Coriolis force can be included in this model. The model is being applied for the several tsunami scenarios and past tsunami events in Mediterranean Sea, and in the Indian Ocean (2004 Sumatra, 2006 Java, and several scenarios) (Tinti & Tonini, 2013; Titov, Tsunami Forecasting, 2009).

In 2002, the Norwegian Geotechnical Institute/ ICG, Norway developed SKREDP. The model is certified and tested with analytical benchmarks. The coordinate system is Cartesian. Any initial sea-surface deformations, prescribed source functions for landslides and earthquakes are inputs of the tsunami source for this model. The model has been applied to northeast Atlantic, to the Arctic and Indian oceans, to Norwegian fjords, and the Mediterranean, and South China seas, as well as to hydropower reservoirs in Norway and the Philippines (Harbitz, et al., 2007).

GeoClaw is a recently validated tsunami model developed by R. LeVeque's Applied Math group at the University of Washington (Gonzales, et al., 2011). It uses a dynamic mesh refinement for an arbitrary number of nested levels. The model uses finite volume, Riemann solvers as numerical schemes and 2D+1 rectangular mesh with adaptive refinement as mesh/grid type. During the calculations, individual grid cells are tagged for refinement, using a criterion such as wave height; thus, disturbed water parcels are gradually better resolved. The flagged cells at each level are clustered into rectangular boundaries, for refinement to the next level. The

model is also robust in calculating wave dynamics in the presence of bores and steep gradients (George & LeVeque, 2006).

The MOST model is used as an operational (real-time) tsunami forecasting tool at NOAA for the Pacific Ocean (Wei, et al., 2008) and is the model used in this dissertation. Examples of the model's forecasting capability are given and explained well in (Wei, et al., 2008) and (Tang, et al., 2012). MOST has ability to track the shoreline by adding new grid points as a function of time. A pre-computed generation/propagation database and selection of a linear combination of scenarios that most closely matches the observational data can be used as initial conditions for a site-specific inundation algorithm. The database contains 246 model scenarios that cover most active subduction zones around the Pacific. It stores all simulations for each solutions of numerical analysis, including amplitudes and velocities for each offshore location (Titov, 2009).

From all of these examples, it is clear that the validation of numerically computed tsunami run-up against observations gathered in real settings is the key. Estimation of tsunami behavior on land is essential for tsunami mitigation and also for designing an optimal community evacuation system along the coast, in the event of such a catastrophe. Furthermore, Synolaks et al., (2008) further argues that no testing of a tsunami run-up algorithm in idealized laboratory experiments can ensure robust model performance, nor can such testing substitute for field data benchmarking.

Even though there are significant improvements in terms of the accuracy and speed of forecasting tsunamis, it is still a challenge to model them, and improvements are desirable. One way forward is through careful numerical case studies of well observed events (field studies) in order to better understand tsunami dynamics and numerical model performance. One such case-study example, and the focus of my thesis, is the 2009 Samoa earthquake and tsunami.

1.6 ISLAND SETTINGS, CORAL REEFS AND AN OUTLINE OF THE THESIS

On 29 September 2009 at 17:48 UTC, an Mw 8.1 earthquake occurred along the Tonga-Kermadec Trench. A complicated fault rupture (outer-rise earthquake) produced bottom deformations and resulted in tsunami waves that generated localized run-ups exceeding 17 m on the island of Tutuila (Fritz, et al., 2011). These waves claimed 34 lives on Tutuila (out of a total 192 deaths for the event) and caused extensive damage around the island. The impact of the tsunami on Tutuila was well documented in surveys, on tide gauges, and on far-field (deep water) pressure gauges. The event has been widely discussed in the literature (Annunziato, 2012, Beaven, et al., 2010, Clark, et al., 2011, Fritz, et al., 2011, Irish, et al., 2012, Lay et al., 2010, Lynett & Lui, 2011, Okal, et al., 2010, Roeber et al., 2010, Thompson, et al., 2011, Zhou, et al. 2012). The tsunami was detected by coastal tide gauges and offshore sea-level sensors located in the Pacific Ocean. The tectonic setting of the Tonga Trench has produced several tsunamis during the past hundred years (Okal, 2011). A similar tsunami occurred, for example, on 26 June 1917, after an earthquake with a magnitude of Mw 8.3, located approximately 100 km south of Samoa (Gutenberg & Richter, 1936).

The 2009 tsunami on Tutuila and environs has become a canonical, but challenging, case study for numerical tsunami models. The island setting, the presence of both barrier and fringing reefs, and the complicated bathymetry and shoreline geometry are all complicating factors of great interest. By studying such an event in great detail, we can learn general lessons about island tsunamis and, in this tropical case, about the role of their surrounding coral structures in the resulting run-up and inundation.

Chapter 2 of this thesis summarizes the existing literature on the role of corals on tsunami dynamics and describes the often contradictory conclusion these studies have reached. Chapter 2

also describes my numerical modeling of the earthquake source, and the subsequent tsunami using the MOST model already introduced above. I describe the Tutuila Island event, and the earthquake that created it. A feature of particular note for this event was pre- and post-tsunami surveys of the damage to the coral structures surrounding Tutuila. The run-up and inundation from this event were also documented in detail at several dozen villages around the perimeter of the island. Chapter 2 also describes my numerical modeling of the earthquake source, and the subsequent tsunami using the MOST model already introduced above. The model results show some skill for simulated run-up variations around the island compared to observations, but overall the MOST model underestimates run-up by an average of 40%. We find no relationship between modeled dynamical fields and coral damage, implying either that there are additional complicating factors that preclude an association, or that the coral-damage survey, although more detailed than any previous study, was nonetheless not comprehensive enough to identify the linkages.

Chapter 3 of this thesis builds on the numerical simulations presented in Chapter 2. Two key factors in modeling tsunami dynamics are studied in more detail: the magnitude of the surface roughness, and the near-shore bathymetry surrounding the island. Reducing the roughness coefficient used in the model can improve the overall simulation of run-up for this event, but the effect is far from uniform for all villages, and for a significant fraction of villages the simulation is actually degraded. In analyses of virtual tide gauges from the model output, I show interesting resonance effects within individual bays. For simulations in which the bathymetry is changed we find the basic results reflect Green's Law - overall, reefs create shallower bathymetry and model simulations show a corresponding increase in wave amplitude. Varying the bathymetry has a strong effect on wave resonance within the bays I studied.

Our results point to several research directions that will be necessary for improved simulations of tsunami run-up and inundation. In the highly heterogeneous littoral and coastal environments, spatial variations in basal roughness will have to be considered, and perhaps a mathematical reformulation of the dissipation terms used in tsunami modeling. The bulk drag formulae used in MOST and many other tsunami models, although possessing the advantages of convenience and simplicity, are a crude representation of the highly sheared turbulent flow at these scales, and their continued use will necessarily limit the predictive capabilities of such models.

Chapter 2. EVALUATION OF THE RELATIONSHIP BETWEEN CORAL DAMAGE AND TSUNAMI DYNAMICS

2.1 INTRODUCTION

Large tsunamis can wreak devastation upon the near-shore environment. There is abundant documentation of the impacts on the subaerial portion of that environment, but much less on the impacts on the submarine portion. In many tropical settings coral reefs form an important component of the submarine environment, being the cornerstone of the local ecosystems, as well as shaping the near-shore bathymetry. There is thus the potential for two-way interactions between reefs and tsunamis. The reef bathymetry influences the tsunami dynamics; and tsunami events may cause significant damage to fragile coral structures. In this thesis we report on a unique opportunity to document tsunami-related damage, and to evaluate whether the damage can be straightforwardly related to particular aspects of the tsunami dynamics.

On 29 September 2009 at 17:48 UTC, an Mw 8.1 earthquake occurred along Tonga-Kermadec Trench. A complicated fault rupture produced bottom deformations and resulted in tsunami waves that generated localized run-ups exceeding 17m on the island of Tutuila. These waves claimed 34 lives (out of total 192 deaths for the event) and caused extensive damage around the island. The tsunami was detected by coastal tide gauges and offshore sea-level sensors located in Pacific Ocean. The tectonic setting of the Tonga Trench has produced several tsunamis during past hundred years (Okal, et al., 2010).

Following the September 29, 2009 tsunami, field surveys were conducted (Fritz et al., 2011) to document the relationship between the physical near-shore environment and the tsunami impact. According to survey results, the tsunami produced a maximum run up of 17m at Poloa on the western coast of Tutuila, 12m at Fagasa on the northern coast, and 10m at Tula on the

eastern coast. The survey team recorded large variations in the impacts of the tsunami along the coastal bays: a wide range of tsunami run-up, wave directions and inundation. The high degree of spatial variability in these various tsunami fields was somewhat of a surprise to scientists studying the event (Fritz, et al., 2011, Okal, et al., 2010, Beaven, et al., 2010, Roeber, et al., 2010), but was clearly established in the field surveys and confirmed by residents.

The impact of this tsunami on Tutuila has proven unusually hard to simulate in numerical models (Beaven et al., 2010, Okal et al., 2010, Roeber et al., 2010, Fritz et al., 2011). The discrepancies between observations and models have been variously attributed to many factors, including the low-resolution bathymetry and topography, the possibility of resonance over the coral reefs, but most importantly, the unusual complexity of the tsunami source mechanism that may have included multiple ruptures of several fault systems at the same time (Beaven et al. 2010). In this study we also perform a simulation of this event, and aim to build upon the experience of these earlier studies: we try to eliminate any bathymetric and topographic discrepancies by using a very high-resolution (10 m) dataset (Lim, et al., 2009); further, we optimize the tsunami source function by calibrating it with direct tsunami observations. Both far-field pressure sensors (DARTs) and near-field coastal sea-level stations (tide gauges) were used to calibrate the tsunami source for this event. We establish good agreement with the near-field tide gauges (Section 3), meaning that it is unlikely that additional details in the source function would impact the simulation.

One challenge of modeling tsunamis in tropical settings such as this are the pervasive barrier and fringing coral reefs, which create tremendous complexity in bathymetry and topography (Figure 2.1). The impact of reefs in tsunami dynamics has been a topic of discussion in the literature. Such analyses point to a complex picture, and conclusions can occasionally appear

contradictory. Baba, et al., (2008) performed numerical simulations of the 2007 Solomon Islands Tsunami to explore the effect of Great Barrier Reef (GBR) on tsunami wave height, using the low-resolution bathymetry and ignoring sea-bottom friction and wave dispersion. The results indicate reefs decrease the tsunami wave height due to the refraction and reflection. Kunkel (2006) performs 1D and 2D numerical modeling of tsunami run-up for an idealized island with barrier reefs around the island, and shows that coral reefs reduce tsunami run up by order of 50%. However, the Kunkel (2006) simulations also suggest the possibility that gaps between adjacent reefs can result in flow amplification and actually increase local wave heights. Fernando, et al. (2005) and Fernando, et al., (2008) lend support to these numerical results: coral reefs protect coastline behind them but local absences of reefs cause local flow amplification due to gaps. Their results are based on field observations, laboratory measurements (Fernando, et al., 2008), and interviews done by local people in Sri Lanka after the 2004 Indian Ocean tsunami. However, their laboratory simulations treated corals as a submerged porous barrier made of a uniform array of rods, which likely oversimplifies the complex structural distribution of coral reefs.

Other studies find no effect, or even suggest the opposite conclusions (Kunkel, et al., 2006). Based on quantitative field observations of coral assemblages at less than 2m depth in Aceh after the 2004 Sumatra-Andaman tsunami, Baird, et al., (2008) conclude that the limit of inundation at any particular location is determined by a combination of wave height and coastal topography, and is independent of the reef quality or development prior to the tsunami. Further, Chatenoux, et al., (2006) perform statistical and observational analysis of 56 sites located in Indonesia, Thailand, India, Sri Lanka and Maldives with a coarse resolution bathymetry and qualitative coral damage data. They find that the higher the percentage of the corals, the larger the

inundation distances behind coral reef on the coast. Lastly, Roeber, et al., (2010) identify strong correlations between the high variability of run-up and inundation along bays at Tutuila during the 2009 Samoa tsunami with the geomorphology of the island, and suggest a role for high concentrations of resonance energy within particular bays. All of these locations of high-energy concentration have fringing reefs extending 100 m to 200 m from the shores. Based on their tsunami simulations, they hypothesize that fringing reefs might amplify near-shore tsunami energy and worsen the impact of short-period dispersive waves.

In this chapter, wave heights, inundation at the coast, and tsunami wave dynamics are simulated for the island of Tutuila for the 2009 tsunami. The simulations are compared with field observations at the coast and wave pressure gauges (DARTs) located around Tutuila to find a relationship between coral damage and coastal metrics of tsunami dynamics. The results contribute to an ongoing discussion about how tsunami dynamics impact corals and how, in turn, that damage might potentially be used to constrain tsunami simulations.

The remainder of the chapter is organized as follows. Section 2 describes the study area, the earthquake and tsunami event, and the observational data sets. Section 3 describes the numerical modeling of the earthquake source and the subsequent tsunami. Section 4 presents an analysis of the relationships among the observational data sets and simulated tsunami fields. We conclude with a Summary and Discussion that suggests an outline for future research directions.

2.2   TUTUILA ISLAND

The study area of my research is Tutuila Island, in American Samoa, the United States' southernmost territory. The Samoa island chain in the central South Pacific Ocean includes five islands, of which Tutuila is the largest and also its center of the government. It is located at roughly 14° south of the equator between longitudes 169° and 173° west (Figure 2.1). The

following will summarize some aspects of the geometry of Tutuila Island that created unique challenges in modeling of the tsunami.

The island formed in the late Quaternary period, from oceanic crust as the Pacific tectonic plate moved over a hotspot (Terry, et al., 2005). Due to its volcanic formation, it has rocky, steep topography and bathymetry, with narrow valleys that rise from ocean floor (McDougall, 1985). The island sits on a shallow submarine platform, which then drops off to a depth of over 3000 m to meet the abyssal plain. Tutuila is approximately 32 km long, with a width that ranges from less than 2 km to a maximum of 9 km. An insular shelf (< 100 m depth) with an average width of 4 km extends along the entire north coast and the southwest region of the island (Figure 2.1).

The island is surrounded by fringing and barrier coral reefs, which contain a diversity of coral reef habitats, and coral species. The island has possibly subsided faster than coral reefs could grow upward, leaving former barrier reefs as submerged offshore banks along the seaward edges of the insular shelf (Birkeland, et al., 2007). Fringing reefs have a width ranging from 0 to 600 m, but 90% of them are less than 217 m (Gelfenbaum, et al., 2011). The barrier reefs are located 2-3 km from the coastline. The total area of coral reefs in the territory of Tutuila is approximately 300 km^2.
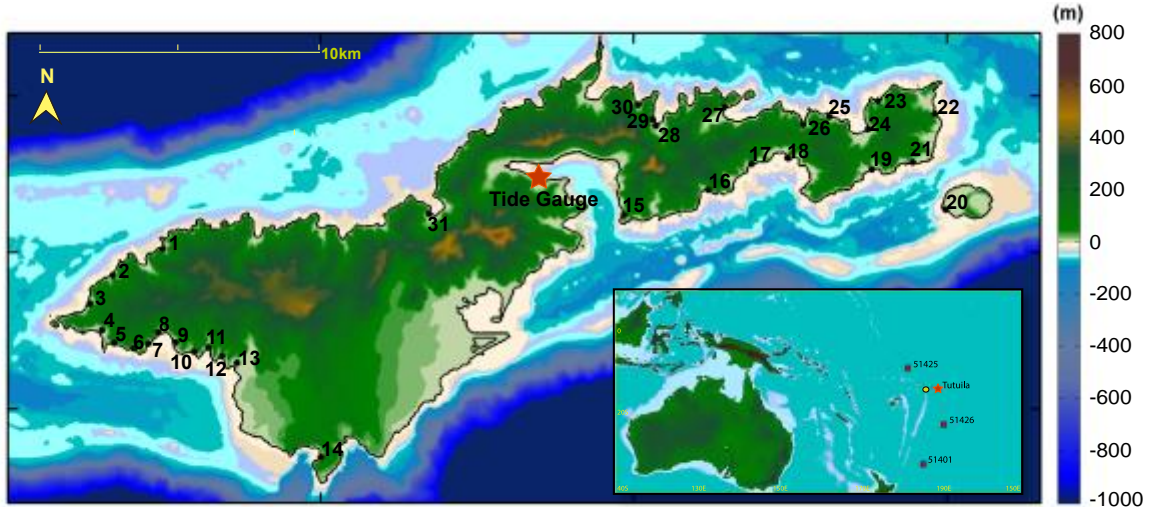
Figure 2.1. Tutuila Island. The black lines around the island on main map indicate the fringing coral damage survey track lines. The beige and light purple colors show the location of the fringing and barrier reefs. The location of Tutuila Island is given as red star on the lower right map. The yellow dot on the same map shows the epicenter of the 2009 Samoa Earthquake. In the inset panel the location of the DART buoys used in optimizing the earthquake fault source used in the MOST simulations are shown. In the main panel, the location of the PagoPago Tide gauge in Tutuila is shown as red star.

2.3   THE SAMOA EVENT

The tsunami from the September 29, 2009 earthquake was generated at the most active region of deep seismicity of Tonga Trench, and reached the Samoan Island chain approximately 20 minutes later. The tsunami caused devastating property damage and loss of life on Tutuila Island, because of its close proximity to the epicenter and the high population density on its coasts.

The cause of the earthquake was the rupture of a normal fault with a moment magnitude of Mw=8.1 in the outer trench-slope at the north end of the trench, near the sharp bend to the west,

followed by two inter-plate ruptures on the nearby subduction zone with moment magnitudes of Mw=7.8 (Lay, et al., 2010). Fault displacements measured by seismic signal, Global Positioning System (GPS) Stations, and ocean-bottom pressure sensors (Beaven, et al., 2010) for these three separate faulting events support this picture. These fault displacements led to vertical movement of the seafloor, and created a complex tsunami source mechanism.

2.4   OBSERVATIONS OF THE EVENT

This particular tsunami afforded a unique opportunity to systematically evaluate the relationship between tsunami dynamics and coral-reef damage. Six months prior to the tsunami, NOAA Coral Reef Ecosystem Division (CRED)-certified divers performed comprehensive surveys of the reefs around Tutuila. The survey lines totaled 110 km in length. Observers measured the number of live, dead, and stressed corals, sea cucumbers, micro-algae, crown of thorns, and urchins along track lines at the depths of 10-20 m. In the immediate aftermath of the tsunami the divers retraced most of the original survey lines. They documented clear evidence of fresh damage at depths between 10 and 20 m. This depth range was selected because of the location of the fore-reef at these depths, which is where the coral population is a maximum. Damage at depths shallower than 10 m was not recorded during the survey (Brainard, et al., 2008).

The divers operated a tow board of instruments as it was tugged behind a boat at a depth of about 15 m. Data taken included direct observations from the diver, a downward facing camera and electronic instrumentation, including GPS (Figure 2.2). The downward-pointed camera recorded the sea bottom habitat. It also captured images at 15 s intervals (NOAA-PIFSC-CRED unpublished data). Selected images of broken and overturned table corals and broken branching corals are presented in Figure 2.2. The survey covered a total of 83 km linear distance within a 5

m horizontal zone either side of the track line. Divers were careful to try to differentiate between damage directly due to the tsunami itself, and land-originating debris entrained into the water.
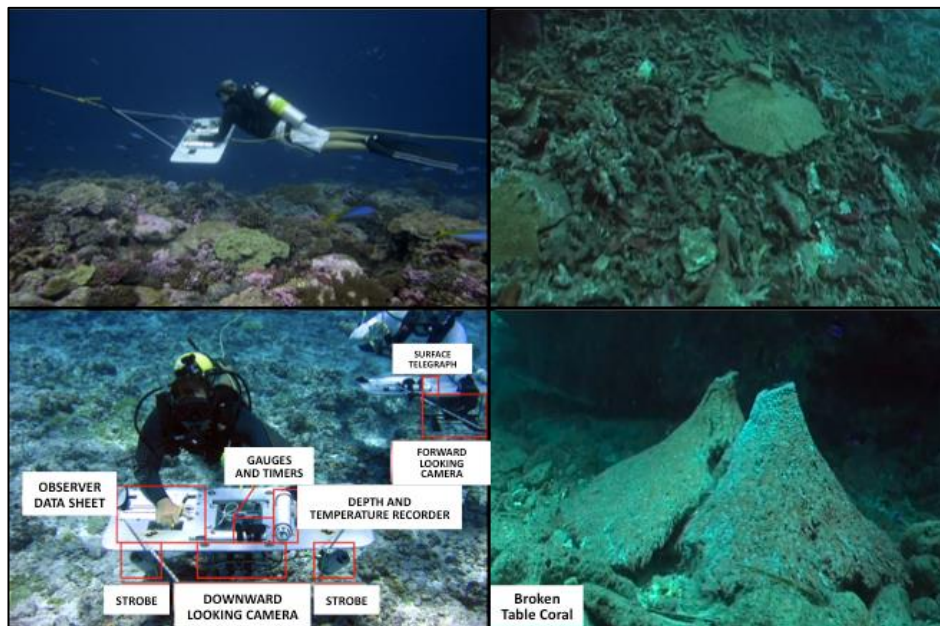
Figure 2.2. Photographs of the coral survey, methods and typical observations. Upper left image shows the NOAA-certified diver surveying a track line with a tow board tugged behind a boat. Lower left image shows the instrument suite on tow boards, among which are observer data sheet, gauges and timers, a camera and strobes. Upper right shows the table and branching corals that have been overturned; lower right shows a table coral that has been broken due to the tsunami. Images are taken from NOAA-Marine Debris Division.

The damage survey report synthesized the direct observations, aggregating track-line data into groupings based on 31 nearby villages, and reported the total number of damage observations. Examples of such summaries are: at Onenoa Village, "coral damage was low, with only one damaged tabulate Acropora sighting was recorded between both divers"; and at

Amaluia Village it "consisted of isolated sightings of broken branching (species of Pocillopora and Acropora) corals". Even though the survey is not an absolute measure of coral damage and involves a degree of subjectivity, it is nonetheless a useful window onto the impact of tsunami dynamics in the immediate aftermath of the event. Since the full coral density of the island is not available, variation in coral density might influence the results (NOAA-PIFSC-CRED unpublished data).

The datasets of the damage collected by the divers are discontinuous and unevenly distributed, and this precludes classifying the data in terms of damage with conventional methods such as standard deviation or equal intervals. Instead we used Jenks Natural Breaks classification method, a univariate version of k-means clustering (Jenks, 1967) by sorting it from lowest value to highest and looking for large gaps, or *natural breaks*. This is done by seeking to minimize each class's average deviation from the class mean, while maximizing each class's deviation from the means of the other classes. In other words, the method iteratively seeks to reduce the variance within the same classes and maximize the variance between classes. The final classification in terms of coral damage is (*0 no damage, 1-27 low, 38-63 medium, 83-159 high, 310 very high damage*). While we felt the Jenks method is most appropriate for this data, our overall conclusions are not sensitive to this choice. An international tsunami survey team observed and recorded tsunami run-up and inundation on the islands of the Samoan archipelago including Tutuila a week after the tsunami (Fritz, et al., 2011). The surveys followed the tsunami survey protocols reviewed by (Synolakis & Okal, 2005). The team marked the values of run-up at 59 different field locations at Tutuila.

2.5   MODELING THE EVENT

2.5.1   *The Model Set-up*

We simulate the 2009 Samoa Event using the MOST Model (Titov & Gonzales, 1997). The primary metrics for comparison with observations are wave run-up and inundation. MOST solves the shallow water equations with a leapfrog finite difference scheme (Titov & Synolakis, 1998). We define three, nested bathymetric and topographic grids. The earthquake dislocation is input as the tsunami source; several predetermined tsunami sources were tried (Zhou, Wei, & Titov, 2012) in order to optimize the agreement with tide-gauge observations. Regional bathymetry and topography datasets (

Table 2.1) were compiled and provided by National Geophysical Data Center (NGDC) and used to create the three nested grids (resolutions of 360 m, 60 m, and 10 m, respectively, see Figure 2.3).

Table 2.1. Sources compiled by NGDC to create the three nested grids (Lim, et al., 2010)

Source of Data	Production Date	Data Type	Horizontal and Vertical Datum	Spatial Resolution (m)
NGDC	1962 to 1998	Single beam echo-sounder		~100
NGDC	2009	Digitized coastline		30
NGDC	1996-2005	Multi-beam Swath Sonar		30-90
Gaia Geo-Analytical	2008	Estimated depths from satellite imagery	WGS-1984 and MHW	~ 5
NAVEOCEANO	2006	Bathymetric-topographic data		5
SCSC	2002	Vector Data		10
USGS	1996-2006	NED Digital Elevation Model		30
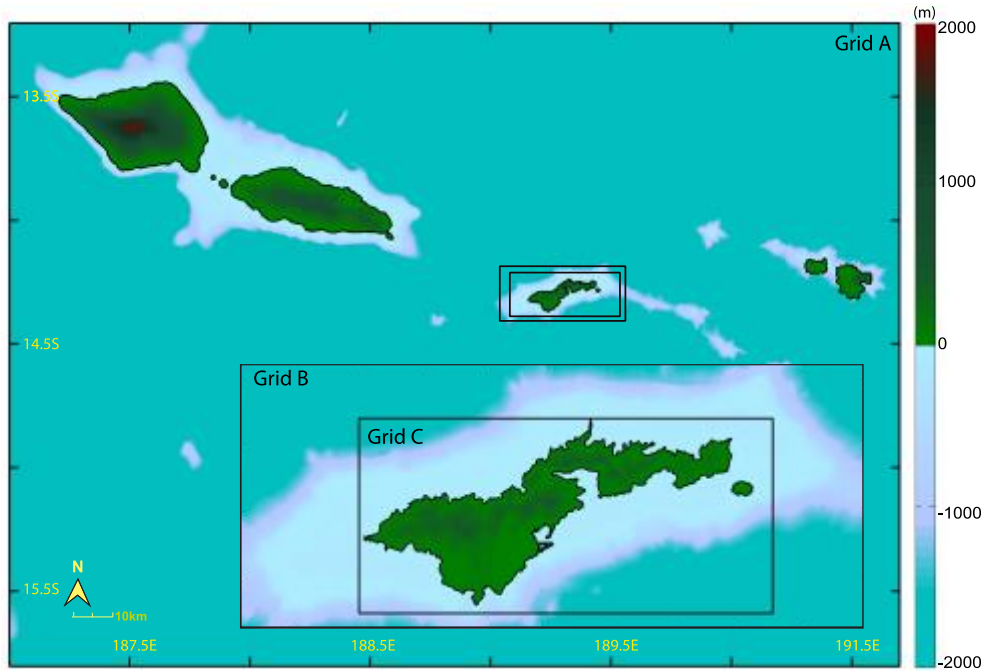
Figure 2.3. The boundaries of the nested A, B and C grids used in the MOST simulations.

2.5.2 *Choice of the Source Function*

We simulated the 2009 Samoa Tsunami with a tsunami source function, *f,* calibrated to direct observations. For this event, several combinations of source functions *f* have been developed for use in previous works (Zhou, et al., 2012; Uslu, Eble, & Wright, 2013; and Liujuan Tang, personal communication, 2009). Earthquakes are modeled as a combination of "unit sources", S_1, S_2, S_3 and so on (Eq. 1.1). Each unit source is a reverse thrust of a given strike, dip, and depth, and each has a moment magnitude of 7.5 (Gica, et al., 2008). The parameters for these unit sources were chosen according to the inversion results of the method described in Gica, et al. (2008). The tsunami source function *f,* is converted into an initial wave height using the elastic model of (Okada, 1985; Okal, et al., 2010). This assumes the rupture of rectangular fault planes cause vertical displacements of the sea floor, and that the initial water level movement is equal

and instantaneous with the corresponding vertical sea-bottom displacement. The inversion finds the linear combination of unit sources that best matches the DART buoy data (Percival, et al., 2011)

We tested four previously optimized source function f. Our choice of source function f was based on optimizing the agreement to the PagoPago tide gauge data. Of the source functions we considered, that of (Uslu, Eble, & Wright, 2013) performed the worst, underestimating wave heights by a factor of four. The other three sources all performed comparably and performed well: for the first four waves, they all matched the tide-gauge wave amplitudes to within about 10%, and the timing of crests and troughs to within 20 minutes. We confirmed our results were robust to the choice of f by simulating time series of wave-height (i.e., 'virtual' tide gauges, Appendix A) at a model grid-point west of the island for each of the fs. The outlier f for PagoPago remained an outlier, and there was close agreement among the other three fs. Although our results would be similar for any of these three fs, we picked the source function with the best agreement to PagoPago for which

$$f = 6.45S_1 + 6.21S_2 \tag{2.3}$$

where the specific parameters of S_1 and S_2 are given in Table 2.2.

2.5.3   *Evaluation of the Model Results with DART and Tide Gauges*

We first compare the tsunami wave amplitudes simulated with MOST to the tide-gauge observations in PagoPago in the near field and three DART Buoys 51425, 51426 and 54410 in the far field regions. For their locations, see Figure 2.1. The simulated amplitudes match fairly well with the recorded values, particularly for PagoPago (Figure 2.4) and particularly the first half-dozen fluctuations. The DART buoys record high-frequency crustal Rayleigh waves in the

hour or so ahead of the arrival of the lower frequency tsunami waves (Figure 2.5). Because the DART buoys lie farther from the source than Tutuila, phase discrepancies are expected to appear, which is particularly evident for DART Buoy 52425 (Figure 2.5a). The discrepancies between the computed and recorded values at the DART buoys are likely also due to a secondary rupture occurred during the earthquake, which has been characterized in the model as one instantaneous rupture of the source function f. However, because of the excellent agreement with the PagoPago tide-gauge observations, we are confident these discrepancies are negligible for the purpose of run-up and inundation computations around Tutuila.

Table 2.2. Parameters of the two tsunami unit source functions, S_1 and S_2 (Eq. 2.1), used to simulate the 2009 Samoa tsunami.

Unit Source	Longitude (°E)	Latitude (°S)	Dip (°)	Rake (°)	Strike (°)	Depth (m)	Mw	L (km)	W (km)	Slip (m)	Scaling parameter (ß)
1	187.2330	16.2754	9.68	90	182.1	5.00	8.1	100	50	1	6.45
2	187.8776	15.6325	57.06		342.4	6.57					6.21

2.6   ANALYSIS

A comprehensive summary of data and analyses are presented in Table 2.3. We first evaluate whether there is any clear relationship between the two main observational datasets for this event – the coral damage and tsunami run up for the 31 village sites. From Figure 2.6 it is visually obvious that no such relationship exists ($r = 0.12$). Even excluding outliers (13 m run up, 100 damage numbers at Vaitogi, 5 m run up and 310 damage numbers at Fagatele) the data still do not yield a clean story ($r = 0.18$). Across a range of run ups between 2 and 8 m, coral damage is as likely to be low or very low, as it is to be high or very high.

Figure 2.4. Comparison of observed (black) and simulated (red) water surface elevations at the PagoPago tide gauge (see Fig. 1) in the four hours after the rupture at t = 0 (17:48:10 UTC, on Sep 29th, 2009). The MOST model estimated a maximum surface elevation of 2.3m at the tide gauge, which agrees well with the recorded value.

We are obviously constrained by the limitations of the data that is available to analyze, but on this basis no clear relationship between observed run-up and coral damage can be inferred. It is not known whether this is because of limitations in the coral dataset (being only a sub-sampling of the reef environment), whether run-up is not the most relevant metric of tsunami dynamics, or whether the occurrence of coral damage is actually driven by many other unknown factors and antecedent conditions.
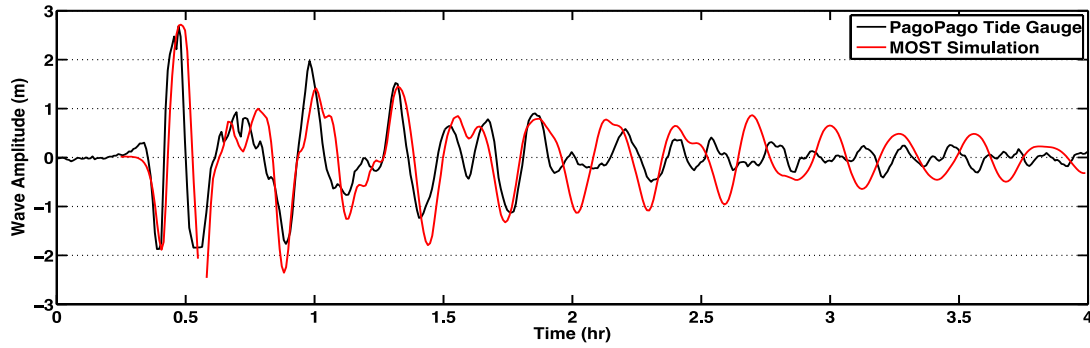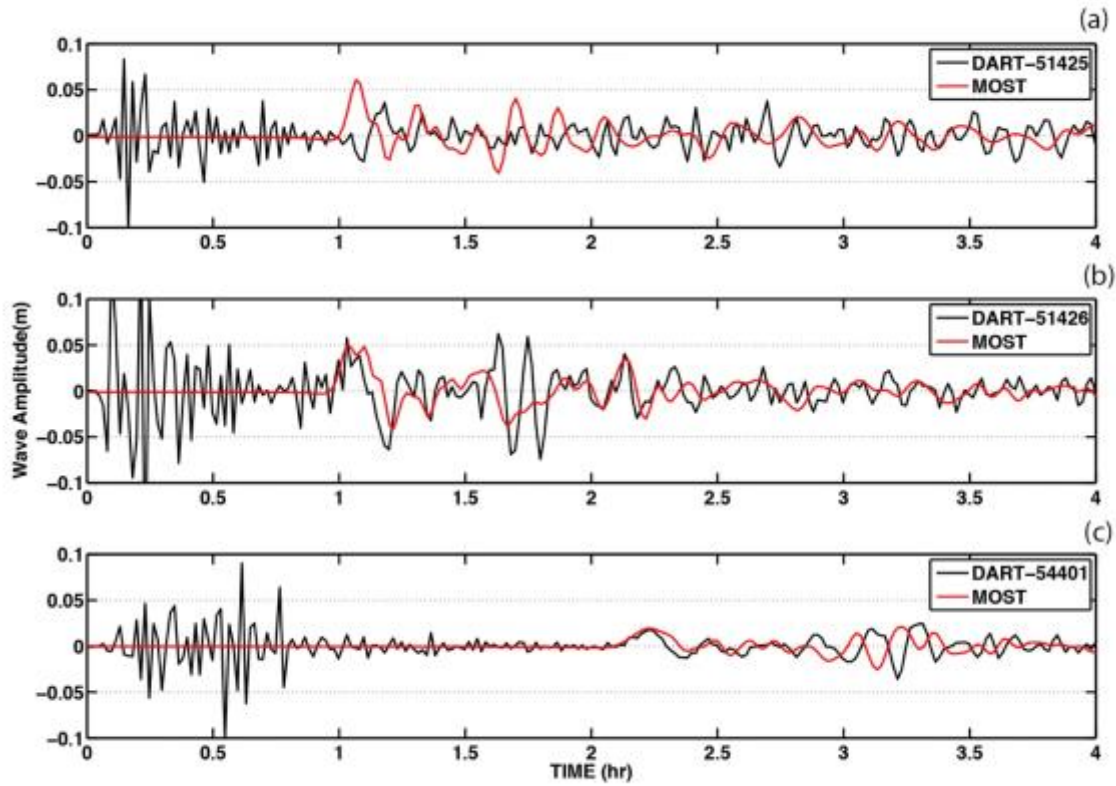
Figure 2.5. A comparison of the observed (black) and simulated (red) water surface elevations at three DART buoys, in the four hours after the rupture at t = 0 (17:48:10 UTC on Sep 29th, 2009): (a) Buoy #51425, (b) Buoy #51426, and (c) Buoy #54401. High frequency, crustal Rayleigh waves are seen ahead of the arrival of the lower-frequency tsunami waves. The MOST model estimated maximum surface elevation of 0.05m at selected DART locations.

Table 2.3. Model, simulated and field run-up, differences, and coral damage at selected 31 villages around Tutuila.

Longitude	Latitude	Village	Model Run-up (m)	Field Run-up (m)	Run-up difference (m)	Difference (%)	Average by Village (%)	Coral Damage	Coral Dam. (numbers)
-170.653	-14.259	AFONO1	3.52	4.31	-0.79	-18.33	-3.05	medium	41
-170.651	-14.26		3.6	4.08	-0.48	-11.76			
-170.653	-14.26		3.9	4.41	-0.51	-11.56			
-170.654	-14.259		3.4	3.75	-0.35	-9.33			
-170.652	-14.26		3.69	3.59	0.1	2.79			
-170.654	-14.258		3.05	2.59	0.46	17.76			
-170.654	-14.257	AFONO2	3	2.25	0.75	33.33	38.43	medium	41

33

Longitude	Latitude	Village	Model Run-up (m)	Field Run-up (m)	Run-up difference (m)	Difference (%)	Average by Village (%)	Coral Damage	Coral Dam. (numbers)
-170.654	-14.258		3.1	2.16	0.94	43.52			
-170.8	-14.332	AFAO	4.2	5.89	-1.69	-28.69	-28.69	low-medium	1
-170.82	-14.331	AGUGULU	2.5	6.12	-3.62	-59.15	-59.15	high	86
-170.659	-14.253	AMALAU	2.12	2.93	-0.81	-27.65	-19.45	no data	no data
-170.658	-14.253		2.13	2.4	-0.27	-11.25			
-170.83	-14.325	AMANAVE	5.25	7.74	-2.49	-32.17	-32.17	high	151
-170.796	-14.33	ASILII	6	6.81	-0.81	-11.89	-11.89	medium	42
-170.792	-14.333	AMALUIA	5.2	5.39	-0.19	-3.53	-3.53	high	116
-170.623	-14.272	AMAUA	3.2	2.91	0.29	9.97	9.97	no damage	0
-170.584	-14.273	AMOULI	3.36	3.38	-0.02	-0.59	1.37	low	13
-170.583	-14.273		3.1	3	0.1	3.33			
-170.585	-14.26	AOA	2.2	2.23	-0.03	-1.35	-1.35	no damage	0
-170.571	-14.271	AUASI	3.08	3.79	-0.71	-18.73	-18.73	medium	38
-170.56	-14.286	AUNU'U	2.14	2.15	-0.01	-0.47	-0.47	high	121
-170.636	-14.28	AVAIO	3.3	3.92	-0.62	-15.82	-3.36	low	14
-170.632	-14.281		3	2.75	0.25	9.09			
-170.826	-14.307	FAGAILII	5.15	5.82	-0.67	-11.51	-18.82	no data	no data
-170.827	-14.307		4.61	6.24	-1.63	-26.12			
-170.725	-14.288	FAGASA	4.2	4.13	0.07	1.69	1.69	no data	no data
-170.81	-14.299	FAGAMALO	3	6.39	-3.39	-53.05	-48.71	no damage	0
-170.81	-14.298		3.5	6.79	-3.29	-48.45			
-170.81	-14.299		3.2	5.78	-2.58	-44.64			
-170.76	-14.365	FAGATELE	3.3	4.92	-1.62	-32.93	-32.93	very high	310
-170.611	-14.27	FAGAITUA	4.75	3.5	1.25	35.71	59.77	no data	no data
-170.615	-14.267		5	2.72	2.28	83.82			
-170.826	-14.329	FAILOLO	2.7	6.54	-3.84	-58.72	-58.72	high	159
-170.787	-14.335	LEONE	2.65	2.75	-0.1	-3.64	67.86	high	83-116
-170.783	-14.336		3.2	0.97	2.23	229.9			
-170.789	-14.336		3.75	4.85	-1.1	-22.68			
-170.631	-14.253	MASEFAU	4	2.96	1.04	35.14	13.02	no data	no data
-170.63	-14.258		4.4	4.84	-0.44	-9.09			
-170.606	-14.259	MASAUSI	3.15	2.79	0.36	12.9	12.9	no data	no data
-170.806	-14.329	NUA	4.2	4.09	0.11	2.69	2.69	no damage	0
-170.582	-14.252	ONENOA	2.6	2.74	-0.14	-5.11	-4.75	no damage	0
-170.581	-14.251		2.4	2.51	-0.11	-4.38			
-170.834	-14.316	POLOA	7.6	17.59	-9.99	-56.79	-44.26	low	24.00
-170.834	-14.315		4.93	10.04	-5.11	-50.9			
-170.834	-14.316		8	12.99	-4.99	-38.41			
-170.834	-14.317		8.5	12.31	-3.81	-30.95			
-170.598	-14.257	SAILELE	2.25	2.95	-0.7	-23.73	-23.73	low	1
-170.812	-14.325	SEETAGA	5.57	5.69	-0.12	-2.11	-2.11	low	5
-170.564	-14.256	TULA	3.8	9.52	-5.72	-60.08	-40.87	medium	63.00
-170.564	-14.256		3.8	7.62	-3.82	-50.13			

Longitude	Latitude	Village	Model Run-up (m)	Field Run-up (m)	Run-up difference (m)	Difference (%)	Average by Village (%)	Coral Damage	Coral Dam. (numbers)
-170.564	-14.256		3.24	6.93	-3.69	-53.25			
-170.566	-14.253		3.79	3.79	0	0			
-170.815	-14.329	UTUMEA	4	4.51	-0.51	-11.31	-11.31	low	13
-170.663	-14.288	VAITOGI	1.8	3.36	-1.56	-46.43	-46.43	high	96
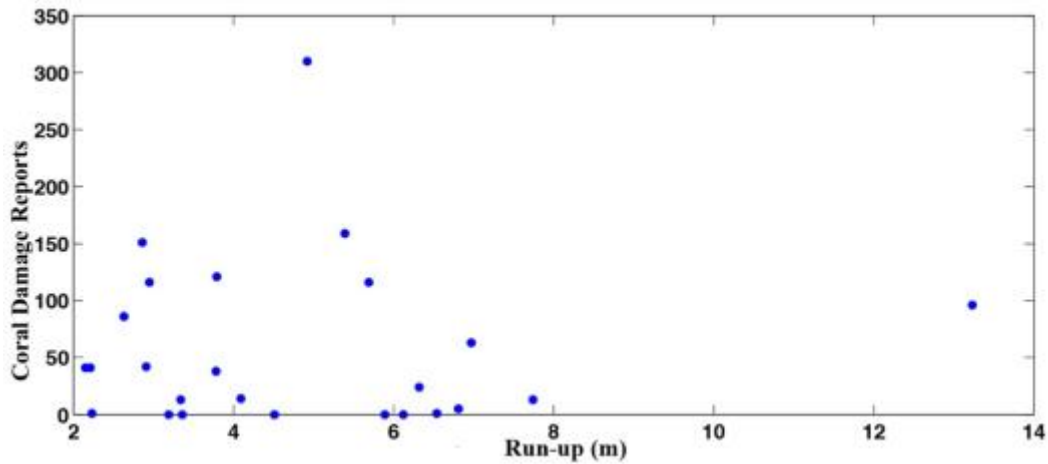
Figure 2.6. Coral damage versus observational run-up. The y-axis shows coral damage numbers reported by the survey team, and the x axis is the average of the run up observations after aggregating the data into 31 separate village locations (see Table 2.3 and Figure 2.1). There is no clear relationship between these two datasets.

We begin by presenting a comparison of the MOST simulations with observations for two representative locations. For the first (Figure 2.7a) in the vicinity of the villages of Amaneve,

Figure 2.7. Two examples comparing observed run-up with MOST run up and maximum wave height. Coastal run up is shown as black bars (observed) and red bars (simulated). Colors show contours of maximum wave height simulated by MOST. (a) the villages of Amaneve, Failolo and Agugulu (locations 4,5, & 6 in Figure 2.1 and Table 2.3)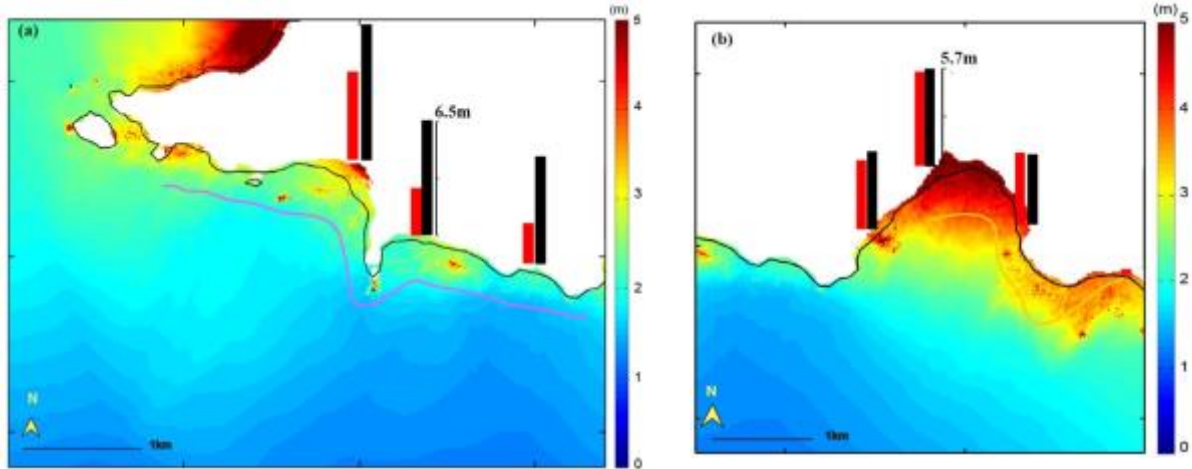; (b) the village of Utumea West, Seetaga and Nua (locations 7, 8, & 9 in Figure 2.1 and Table 2.3). The survey tracks nearest these villages are also shown, color-coded according to the damage scale in Figure 2.10

Failolo, and Agugulu (4, 5, and 6 in Figure 2.1), observed run up averaged 8 m. The MOST model does poorly, underestimating the run up by an average of 45%. This was a region where high coral damage was documented. For the second (Figure 2.7.b), near the villages of Utumea West, Nua and Seetaga (7, 8 and 9 in Figure 2.1) average run up was 4 m. Here the MOST model does well, simulating run up to within 2.4%. The documented coral damage was very low. Even though these two locations are only 3 km apart, these very different run ups, coral damage, and simulation performance illustrate the complexities of the setting.

Figure 2.8 shows some of the dynamical fields simulated by MOST for this event: maximum wave amplitude (panel a), maximum current (panel b), maximum momentum flux

(panel c) and peak stress (panel d), respectively, together with the coral damage along the survey tracks. From a visual analysis, there are not obvious strong relationships between coral damage and tsunami dynamical fields. Take just two examples, Leone and Fagatele (13 and 14 in Figure 2.1): at Fagatele the maximum flux, current and maximum amplitudes are low, but coral damage is very high. In contrast, at Leone, the maximum flux is high with low maximum amplitudes and currents, and high coral damage.
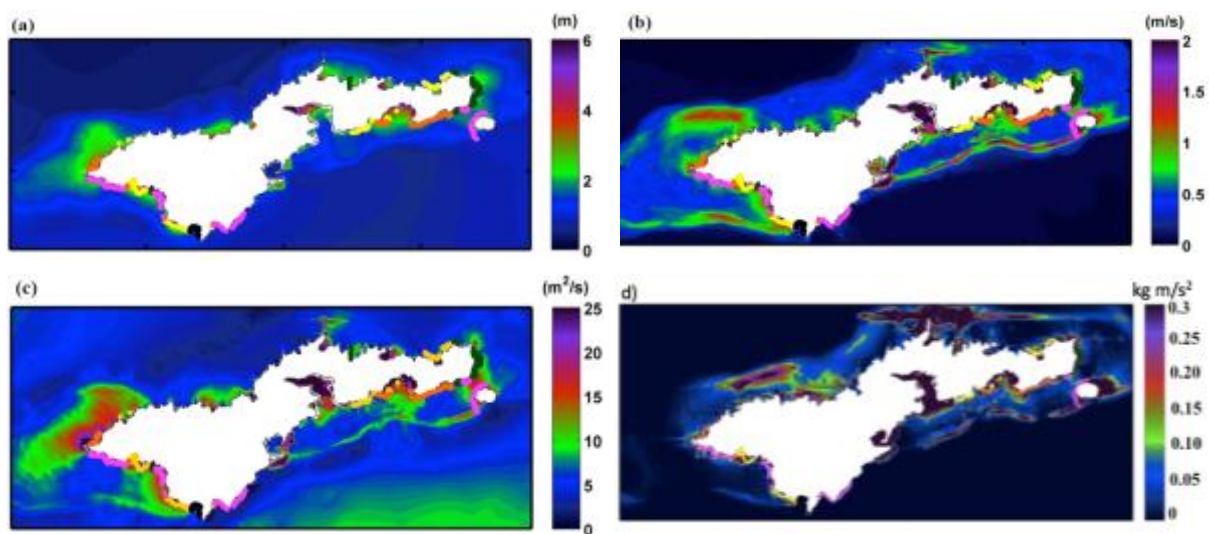
Figure 2.8 Maximum wave amplitudes, peak currents, peak momentum fluxes and maximum stresses calculated from the MOST simulation of the 2009 Tutuila tsunami. Also shown are the post-tsunami survey tracks with coral damage according to the color scale in Figure 2.10.

The absence of a statistically significant relationship between the modeled tsunami fields and the observed damage is confirmed by averaging MOST output along each survey track and creating scatter plots of observed damage vs. track-averaged model output, for several relevant model fields (see Appendix A).

The clearest basis that we identify for comparing the observations and the model is the observed coral damage and run-up, and the simulated run up, at each of the 31 sites where observations were made. Table 2.3 compiles the complete results from all the available observations. We have aggregated the observed and computed run-up values into reports at 31 villages by taking the mean of the total data points at every village. The complete data set for the whole island is presented graphically in Figure 2.9 and in Figure 2.10. A scatterplot of simulated vs. observed run up correlates at r = 0.78, demonstrating significant overall skill for the MOST model (Figure 2.9). Despite this success, it is also clear MOST underestimates in many places. Of the 31 total villages, there are 15 for which MOST underestimates run up by more than 10 percent. Figure 10 shows the bulk of these are on the west side of the island, although not exclusively so. At only 5 villages was the run-up overestimated by more than 10%. Therefore, at the remaining 11 villages the model simulated the observed run up to within 10%. Thus, while the nearby tide-gauge observations are well simulated by MOST (Figure 2.9) there is an overall tendency for MOST to underestimate run-up for this event.

Turning to the coral damage reports for these villages, the data is suggestive of a general relationship with the accuracy of the run-up simulations (Table 2.3). Of the 15 villages where the model under-estimated the run up, the breakdown in terms of coral damage is 8 *very high/high*, 4 *medium, 3 low/very low,* 1 *no damage,* 1 *no data.* For 11 villages where the model estimates run up well the coral-damage is 2 *very high/high*, 1 *medium*, 3 *low/very low*, 4 *no damage*, 1 *no data*.
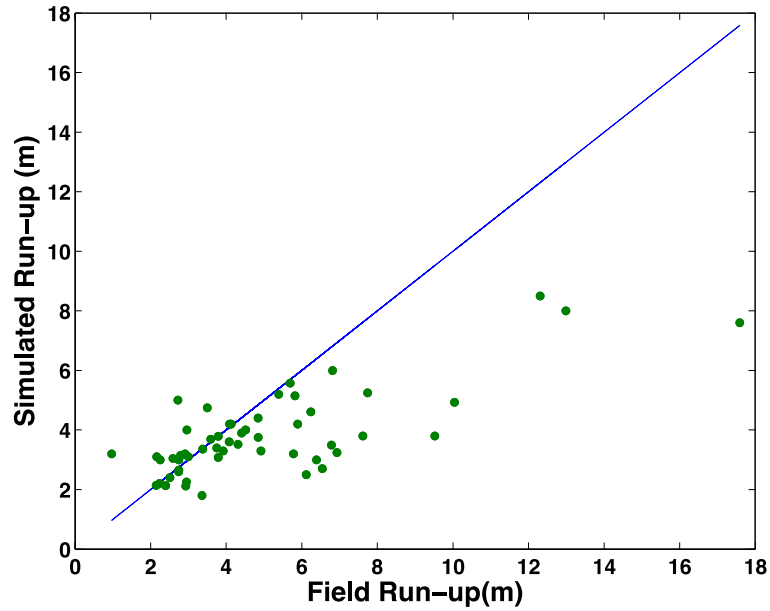
Figure 2.9. Scatter plot of simulated versus observed run-up (m). The blue line shows the 1-to-1 line. The simulated vs. observed run up is correlated at r = 0.78 (Pearson product-moment calculation coefficient), but MOST underestimates run up at many places.

For the 5 villages where run-up is overestimated, limited coral-damage data precludes strong interpretation, 1 *high*, 1 *medium*, 3 *no data*. We expected to see a relationship between coral damage and tsunami dynamics since damage is directly relevant with tsunami energy and this with the dynamics of waves.
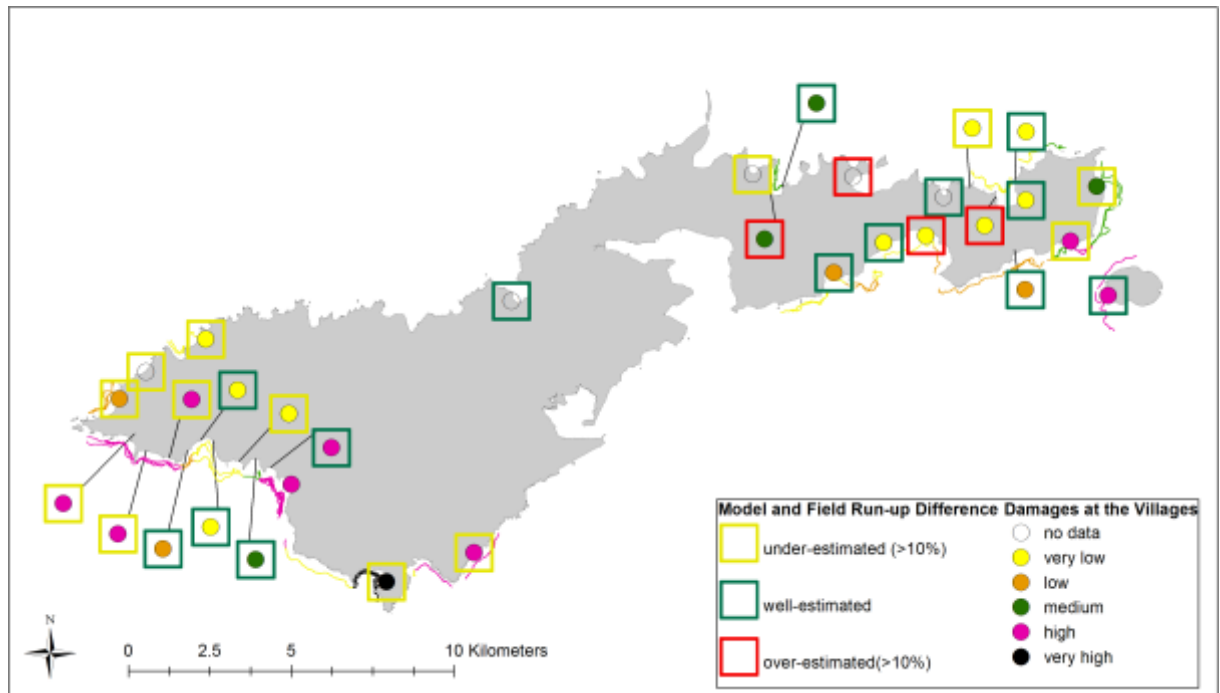
Figure 2.10. A summary of the comparison between model run-up skill and coral damage where. Rectangles indicate the difference between modeled and observed run ups. The filled dots indicate the coral damage reports using the qualitative classification described in the text. Lines are the color-coded survey track-lines followed to estimate the damage on corals.

See also Table 2.3

2.7   SUMMARY AND DISCUSSION

Focusing on the impact of the 2009 Samoa tsunami on Tutuila Island, we conducted numerical model simulations of tsunami run-up and inundation at the coastal zones. We performed an integrated analysis to evaluate the relationship between the tsunami hydrodynamics and the coral damage by using numerical modeling and post-tsunami surveys. The results for 31 villages on Tutuila island suggest that, while the numerical model simulates run-up with a high correlation to the observations, there is also a tendency to underestimate run-up in regions of high or very high coral damage, and that run-up tends to be better estimated in locations where coral damage is low.

The dataset synthesized in Table 2.3 is a preliminary assessment of the damage to the fringing reef coral. Although the 2009 Tutuila tsunami was a one-of-a-kind opportunity to investigate coral damage and tsunami dynamics, the data has some limitations. In particular, the damage assessments inevitably involve a degree of subjectivity and the damage reports have not been normalized to the background coral density. Moreover, the data covers only the east and west side of Tutuila due to the bad weather conditions that existed on the south and north side of the island during the surveys.

In the present setting of Tutuila island, the variable simulated run-up differences in our high-resolution tsunami model might be due to sharp changes in bottom roughness values caused by coral reefs. One expects that in reality there are strong spatial variations in roughness values (Nunes, et al. 2008). However, a constant roughness value was defined in the MOST simulations. To our knowledge, this is a limitation shared by most current tsunami models. A model sensitivity analysis simulating the effect of varying the depths where coral reefs exist may better elucidate their role in controlling run-up on the coastlines they shield.

41

While we have found some intriguing relationships between tsunami dynamics and coral damage, at least in the spatial variations in the skill of the numerical simulations, it is clear these are only tentative gleanings amid a great deal of variability. We did not find any clear relationships between coral damage and other simulated dynamical tsunami fields. Such relationships might be drawn out in more targeted and more detailed simulations, but the real situation is obviously very complicated at small scales, and many factors operate. The failure to establish a stronger connection between the simulated dynamical tsunami fields and coral damage may be because the coral-damage dataset was not comprehensive enough; or because the MOST model does not represent the correct spatial scales in roughness or bathymetry, or the MOST model does not represent the processes that actually cause damage (for instance, damage may be inflicted on corals by retreating waves carrying debris and sand); or because coral damage is inherently stochastic and unpredictable, and depends unknowably on antecedent conditions. Since so little is known about the damage to coral reefs by tsunamis, more studies are needed to examine the influence of water depth, three-dimensional effects, wave-wave interactions and coral strengths.

In some ways it is discouraging to find no correlation between the run-up and coral datasets. On the other hand, it is important to establish that result, and it also points to new questions. The documentation of the submarine ecological impacts of a tsunami is an important goal in its own right, but the tentative inference from our study (the first of its kind) is that the relationship of coral damage to a variety of tsunami metrics (i.e., observed run-up and inundation, modeled maximum currents, fluxes, and stress) is not a simple one, at least in our setting. Tutuila represented a 'target of opportunity', since the all-important pre-tsunami survey existed. Therefore, understanding in more detail the impact of two important controls: magnitude of the

roughness and the near-shore bathymetry, is the research subject of the following chapter in understanding impact of reefs on tsunami run-up and inundation results.

Chapter 3. THE ROLE OF CORAL REEF ROUGHNESS AND BATHYMETRY ON TSUNAMI DYNAMICS; CASE STUDY: 2009 SAMOA TSUNAMI

3.1   INTRODUCTION

It has proven difficult for numerical simulations of 29 September 2009 Samoa tsunami event to successfully reproduce the large variations in tsunami run-up and inundation among the many coastal villages where observations were made. One challenge for numerical tsunami models in tropical settings such as this is to properly simulate the impact of the pervasive barrier and fringing coral reefs (Figure 2.1). In many respects, the 2009 Samoa tsunami serves as a benchmark event for tsunami numerical modeling experts to test their models in a complex submarine environment and to better understand tsunami risks for island communities like Tutuila, around the world.

In Chapter 2 of this dissertation, we showed that numerical simulations had some predictive skill but overall the model tended to underestimate run-up by about 40%; we also showed that there was a high degree of variability in simulated run-up even among adjacent bays. The work further suggested that understanding in more detail the impact of two important controls, roughness and bathymetry, would be a useful next step in understanding the impact of reefs on tsunami dynamics.

In this chapter, we investigate the effects of reef roughness and reef bathymetry on Tutuila Island. We focus on two main goals: firstly, we want to understand how roughness variations affect run-up and inundation; secondly, we perform a model sensitivity analysis varying the bathymetry where fringing coral reefs exist to elucidate their role in controlling run-up on the coastlines they shield.

The remainder of the chapter is organized as follows: Section 2 presents the analyses of this chapter. Section 3 is the summary and discussion.

3.2   ANALYSIS

3.2.1   *The Impact of Changing Manning's Roughness, n*

In the MOST numerical model, the effects of bottom friction are implemented by incorporating a basal shear stress with components (τ_{xz}, τ_{yz}) into the shallow water equation and parameterized by a drag formula:

$$(\tau_{xz}, \tau_{yz})/\rho = -C_B \frac{\sqrt{U^2+V^2}}{D}(U,V) \quad ,$$ (3.1)

where *U*, *V* are the components of the velocities, *D* is the fluid depth, ρ is density (Titov, et al., 2003) C_B is a dimensionless friction coefficient, which can in turn be related to Manning's roughness parameter, *n,* as:

$$C_B = \frac{gn^2}{D^{1/3}} .$$ (3.2)

The concept of Manning's roughness was originally developed for open channel flow. Manning's *n* values have been measured empirically for a wide variety of different materials in laboratory experiments (Chow, 1959), and by large-scale field studies of river flow for fully turbulent conditions (Bricker, et al., 2015). From Eq. (3.1), C_B is depth-dependent, with increasing depth implying decreased friction. For example, for n=0.025 s m$^{-1/3}$, $C_B = 0.006$ for $D = 1$ m, but $C_B = 0.0025$ for $D = 15$ m. Bottom friction typically has the greatest impact at depths of 0−10 m, and is negligible for tsunami propagation in the deep ocean (Levin & Mikhail, 2016). The simple form of *n* and its relatively straightforward implementation within shallow-water equations has led to its

widespread adoption in tsunami modeling (Imamura, et.al, 2008) for the representation of frictional dissipation of tsunami energy in coastal zones, for both the submerged and subaerial portions of the domain. In many studies, a value of $n = 0.025$ s m$^{-1/3}$ has been adopted as appropriate for a smooth sea bottom or land. A range of other values has also been suggested from $n \sim 0.01$ to 0.1 s m$^{-1/3}$ depending on the setting and basal conditions (Kunkel, et al., 2006); (Tang, et al., 2009); (Jaffe, et al., 2010); (Gelfenbaum G. , et al., 2011) and (Bricker, et al., 2015).

In Chapter 2 of this thesis, we selected $n = 0.03$ s m$^{-1/3}$. Both far-field pressure sensors (DARTs) and near-field coastal sea-level stations (tide gauges) were used to calibrate the tsunami source for this event. Simulated wave amplitudes matched well with tide-gauge observations. However, the comparison of simulated and observed run-up for 31 villages in Tutuila revealed that MOST underestimates the run-up at 15 village sites for this event.

In this part of the research, we first evaluate whether a different value of n can decrease the discrepancy between simulated and observed run-up at selected 31 villages. For some villages, several separate run-up observations were made. For such villages we took the average of all run-up observations. In the MOST model, we took the highest value of computed run-up within a 3x3 grid box (30 m x 30 m) around the locations of each of the observations, and averaged them. We also tried taking the highest value of computed run-up around the locations of all observations and compared this value with the highest value of the run-up observations at that village. Finally, we tried taking the value of computed run-up at the exact locations where we have run-up observations without averaging them and concluded that our results are not sensitive to which of these various methods we use for selection of simulated run-up.

We performed MOST simulations varying n from 0.01 to 0.1 s m$^{-1/3}$, where the lowest n value represents an essentially smooth reef. For $n = 0.01$ s m$^{-1/3}$, although the simulations could be

completed, the MOST model exhibited clear signs of numerical instability in the simulations (grid-point noise and unphysical wave heights), and therefore we do not present those results. In Figure 3.1, we present the remaining simulations for varying *n* as a scatterplot of observed vs. simulated run up at 31 villages around Tutuila. Locations of the villages are shown in Figure 2.1. A comprehensive summary of data and analyses is presented at Table A1.
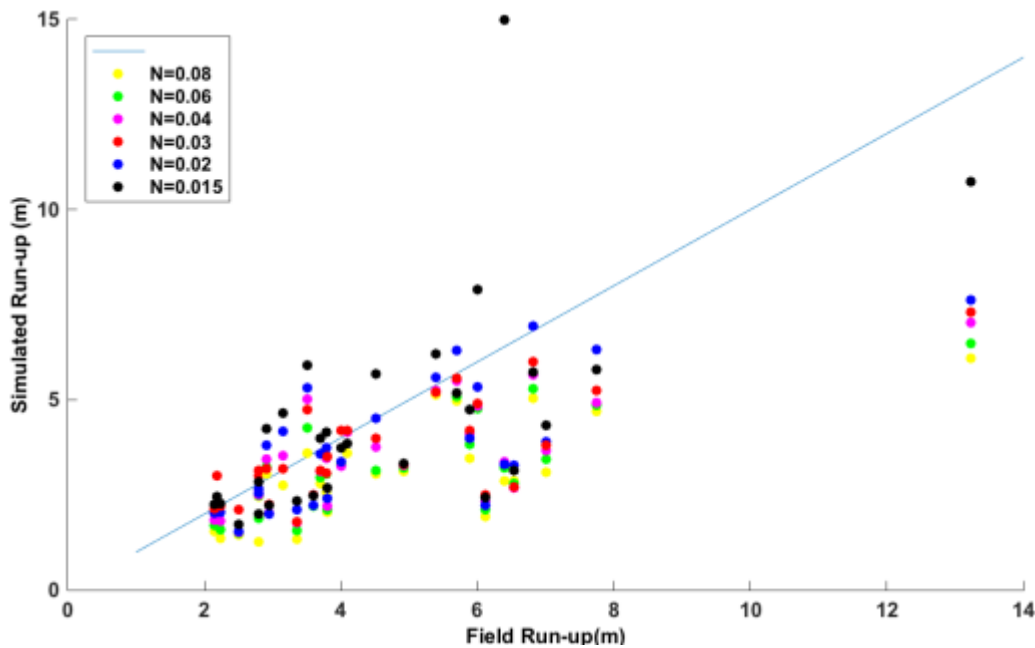
Figure 3.1. A comparison of model and field run-up for the simulations with varying *n* at 31 villages in Tutuila Island. The blue line shows the 1:1 line. Points falling on or close to the blue line show where there is good agreement between simulations and observations.

Overall, for most of the villages, the variation of run up with *n* is straightforward, with higher values of *n* having less run-up. For some villages however, the relationship is not monotonic, and the highest simulated run-up does not always occur for the lowest value of *n*. Thus, at individual locations, the complex patterns of refraction and reflection, and nonlinear interactions can complicate the relationship between dissipation and run-up. This is also clear

from the different spread among the simulated run-ups for different values of *n* at individual villages. At some villages there is very little spread in simulated run-up values as *n* varies (e.g., Fagatele village, observed run-up = 4.92 m, the spread is 4% of the mean simulated value), whereas at others the spread is large (e.g., Poloa village, observed run-up = 13.5 m, the spread is 76% of the mean simulated value).

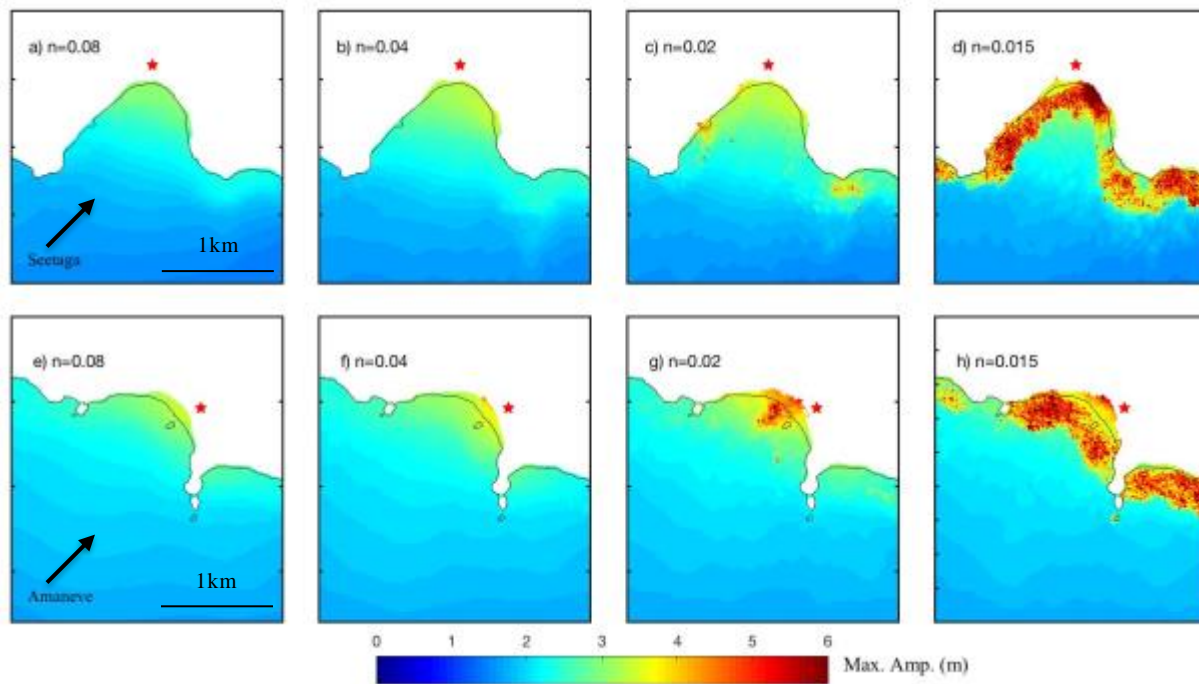Figure 3.2. Simulated maximum wave amplitudes are shown for the bays near the villages of Seetaga (top panels) and Amaneve (lower panels) for n = 0.08, 0.04, 0.02 and 0.015 s m$^{-1/3}$. The pre-tsunami shoreline is shown as a thin black line. Colors inland of that line therefore show the degree of inundation. Village locations are shown as red stars. Black arrows indicate tsunami direction from its source.

The results are mixed with regard to whether different values of n improve the simulated run up compared to observations. The model estimation of run-up is improved by changing n for some villages and doesn't change significantly at others. Of the total 31 villages, at 10 villages the difference between observed and estimated run-up is smallest when $n = 0.02$ s m$^{-1/3}$. At 9 villages the closest match occurs for $n = 0.03$ s/m$^{1/3}$. At 5 villages the closest match occurs for $n = 0.015$ s m$^{-1/3}$. For the remaining 6 villages, two villages each achieve the closest match to observations when $n = 0.04$ s m$^{-1/3}$, $n = 0.06$ s m$^{-1/3}$, and $n = 0.08$ s m$^{-1/3}$.

In our simulations, n is uniform throughout the model domain, which obviously does not capture the real situation of a heterogeneous littoral and coastal environment. Equations (3.1) and (3.2) represent dissipation in these environments. An obvious next step in tsunami modeling is to evaluate whether variations in basal conditions might be represented by spatial variability in n. Introducing spatial variations in n would add tunable degrees of freedom in the model, and in practical applications it would be important not to over-constrain a model. Nonetheless, evaluating whether spatial variations in n might be optimized to provide agreement with detailed measurements in case studies such as ours would represent a `best-case' for the ability of equations to simulate run-up in these events.

Next we evaluate the spatial patterns of the maximum tsunami amplitudes for two representative villages, Seetaga and Amaneve, as a function of n. In Chapter 2, we showed that, for standard parameters ($n = 0.03$ s m$^{-1/3}$), MOST successfully simulated the run-up observations at Seetaga, agreeing to within 2.4%. On the other hand, just 3 km southeast from Seetaga, MOST did a relatively poor job for the village of Amaneve (MOST underestimated observed run-up by 45%). This very different simulation performance illustrates the complexities of the setting, and thus

makes Seetaga and Amaneve suitable to use for the comparison of case studies for change in n and reef bathymetry.

The simulated maximum wave amplitude fields are shown in Figure 3.2a-d for Seetaga, and in Figure 3.2e-f for Amaneve. For Seetaga, $n = 0.03$ s m$^{-1/3}$ provides the best agreement in run-up (5.69 m observed, 5.57 m MOST), whereas for Amaneve, $n = 0.02$ s m$^{-1/3}$ gives closest agreement (7.74 m observed, 6.32 m MOST). For higher values of n, the wave amplitude fields vary smoothly on scales of a few hundred meters, with the highest values of run-up are found in the center of both bays, suggesting a refraction or focusing of wave energy there. As n is reduced from 0.04 to 0.02 s m$^{-1/3}$, some significant localized increases in wave amplitude and inundation appear, particularly in Amaneve bay, where wave amplitude approaches double that of the $n = 0.08$ s m$^{-1/3}$ simulations. For $n = 0.015$ s m$^{-1/3}$ wave amplitudes have increase throughout each bay, and the increases are clearly co-located with the clusters of near-surface reef structures that are dotted around the perimeter of each bay, and which can be seen in detail in Figure 3.3a and Figure 3.3c. Figure 3.2 also shows evidence that lower values of n have some impact offshore with a more complex wave pattern and more small-scale structure, perhaps indicating more scattering of wave energy and a cascade to smaller scales.

We next turn to a comparison of water surface elevations estimated for shallow-water virtual tide gauges near the coasts of Seetaga and Amaneve, for varying n (Figure 3.3b-d). At these villages, the wave amplitude maximizes during the first surge. For the Seetaga tide gauge, the maximum water elevations are 3.1, 3.2, and 3.3 m for $n = 0.08$, 0.04, and 0.02 m s$^{-1/3}$, respectively (Figure 3.3b) At Amaneve, the maximum water elevations are 3.1, 3.4, and 3.9 m for $n = 0.08$, 0.04, and 0.02 m s$^{-1/3}$, respectively (Figure 3.3d). The various values of n do not affect the timing of the waves, and have most impact on the amplitude of the first wave.

Both Seetaga and Amaneve tide gauges show some evidence of resonance or constructive interference between approaching and receding waves (Figure 3.3). We generally expect successive wave heights to decrease in amplitude after several waves, but at both sites wave elevations increase between the fourth and sixth waves then decrease again after the seventh wave. At the tide gauge close to Seetaga, after the third wave, approaching and reflecting waves from the reefs interfere and form constructive superposed waves. Another intriguing thing to see at the Amaneve virtual tide gauge is that the tsunami waves drop off in amplitude more quickly than at Seetaga and have a less sinusoidal form. By 1.5 hr after the first waves, the tsunami has become a distorted noisy wave-train. This behavior indicates more nonlinearity and more overall dissipation, compared to Seetaga, perhaps because of the more complicated reef structures within the bay that cause the waves to be dispersed in the reef areas (Figure 3.3a compared with Figure 3.3c).
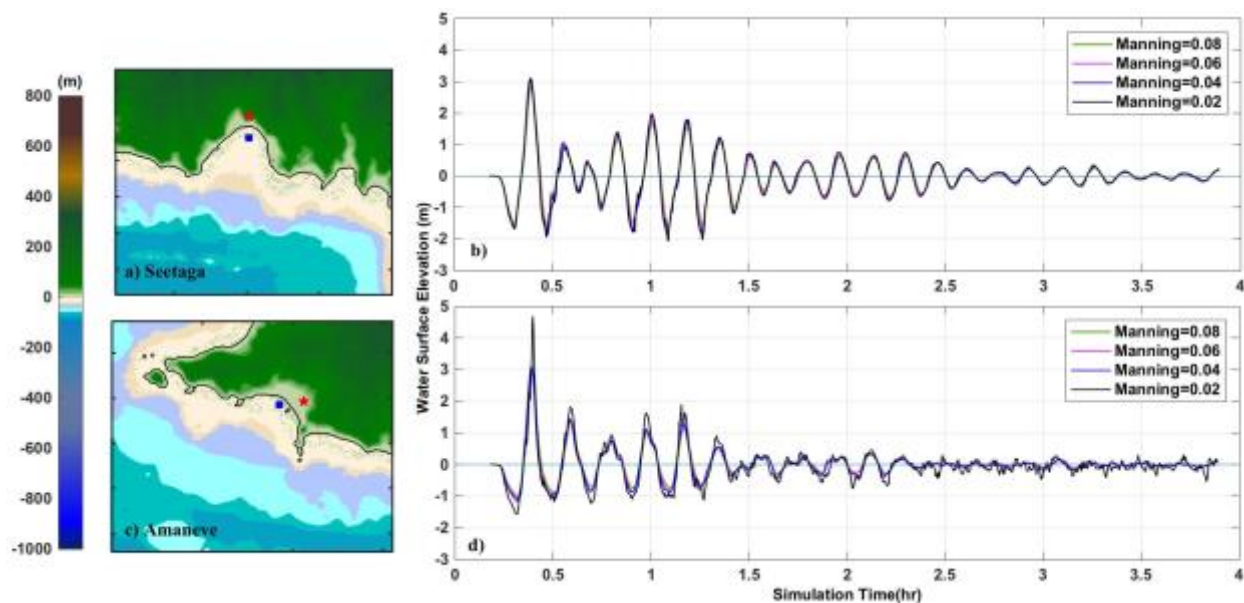

Figure 3.3. Comparison of water surface elevations at selected virtual tide gauges in the near-shore regions of villages of Seetaga (Fig. a-b) and Amaneve (Fig. c-d). Maps show the location of the

villages as red stars, and the locations of the virtual tide gauges are shown as blue square. In b) and

d) water surface elevations are given for varying n during the 4 h after the fault rupture at $t = 0$

3.2.2   *Changes in Reef Bathymetry*

In this section, we evaluate how variations in coral reef bathymetry affect the tsunami run-up and inundation limits inside the bays at the 31 villages around Tutuila. We generate synthetic bathymetries for the B and C grids by first removing all bathymetry with less than 90 m depth (i.e., bathymetry in the range 0 to 90 m is set equal to 90 m). Let $z_{real}(x, y)$ be the real bathymetry and let $z_{flat}(x, y)$ be the extreme flattened bathymetry. We performed several experiments varying the bathymetry smoothly between these limits using the parameter, r, in the following equation:

$$z_{expt}(x, y) = r z_{real}(x, y) + (1 - r) z_{flat}(x, y) \tag{3.3}$$

Thus, $r = 1$ corresponds to the real bathymetry and $r = 0$ to the flattened bathymetry. We varied r from 0 to 1 in increments of 0.2. The resulting bathymetries are shown in Figure 3.4. In all simulations, a value of Manning's roughness of $n{=}0.03$ m s$^{-1/3}$ has been implemented.

We first focus on maximum wave amplitudes in the MOST simulations with these varying bathymetries implemented.   The wave-amplitude fields near Seetaga and Amaneve are shown in Figure 3.5 and the results for simulated run-up for villages around Tutuila are given in Table A2. In general, we find that wave amplitudes and run-up are smaller when the reef bathymetry is removed, contrary to the common belief that reefs protect reef-surrounded coasts from tsunamis (Baba, et al. 2008, Kunkel, et al., 2006). When there is no reef ($r = 0$), the tsunami run-up achieves its lowest value at 22 out of the 31 villages. For the remaining 9 villages, 4 villages achieve the smallest run-

up when $r = 0.2$, 2 villages achieve the smallest run-up when $r = 0.4$, and 3 villages achieve the smallest run-up when $r = 0.6$ (Table A2).
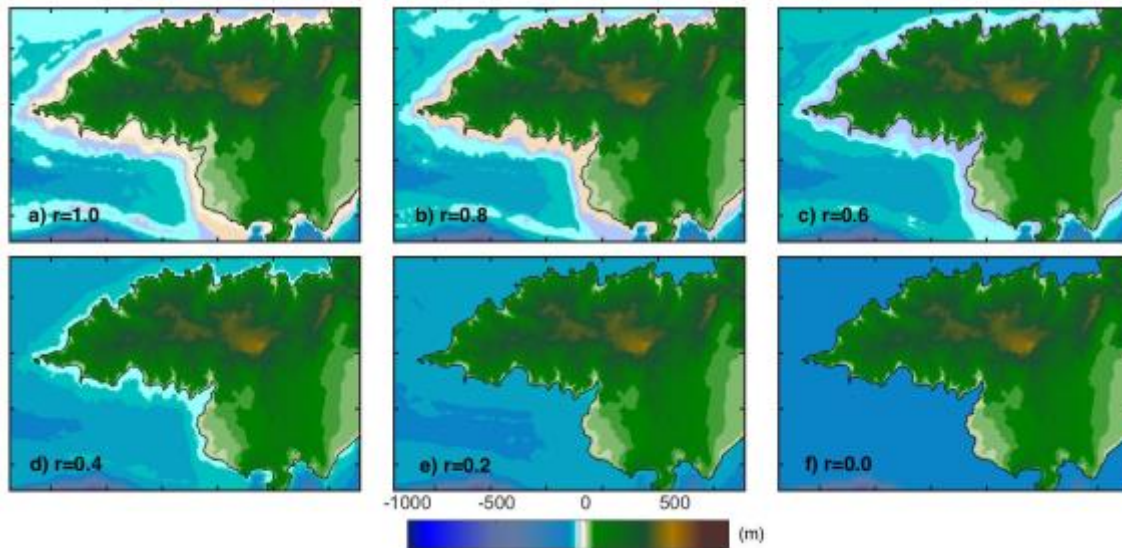
Figure 3.4. C grids of synthetic bathymetry generated from Eqn. 3, shown for the west side of Tutuila Island. $r = 1$, original bathymetry, $r = 0$, no reefs from 0 m to 90 m depths.

The same basic behavior is observed in the maximum wave amplitude fields near Seetaga and Amaneve (Figure 3.5). Wave amplitudes are larger for the real reef bathymetry than for the flattened bathymetry. The MOST model estimates the maximum water surface elevations at Seetaga village as 3.2, 2.2, and 2.1 m for $r = 1.0$, 0.8, and $r = 0.0$, respectively. At Amaneve, the maximum water surface elevations at the tide gauge are 3.4, 2.8, 2.1 m for $r = 1.0$, 0.8, and 0.0, respectively.

These simulations are most simply explained as a manifestation of Green's Law; wave amplitudes increase when reefs are present because of the shoreward-shoaling bathymetry, and the extra dissipation occurring over the shallower depths is not enough to offset this basic tendency. When the reefs are removed, the impinging tsunami waves encounter more of a wall, and are

predominantly reflected rather than dissipated. The inundation limits can be seen in Figure 3.5 from the color shading that lies inland of the pre-tsunami shoreline. It is interesting to note that the inundation limits are not a strong function of the offshore bathymetry, despite the very large variations we've implemented. It suggests that inundation is determined more by the coastal geometry than the tsunami wave dynamics in these bays.
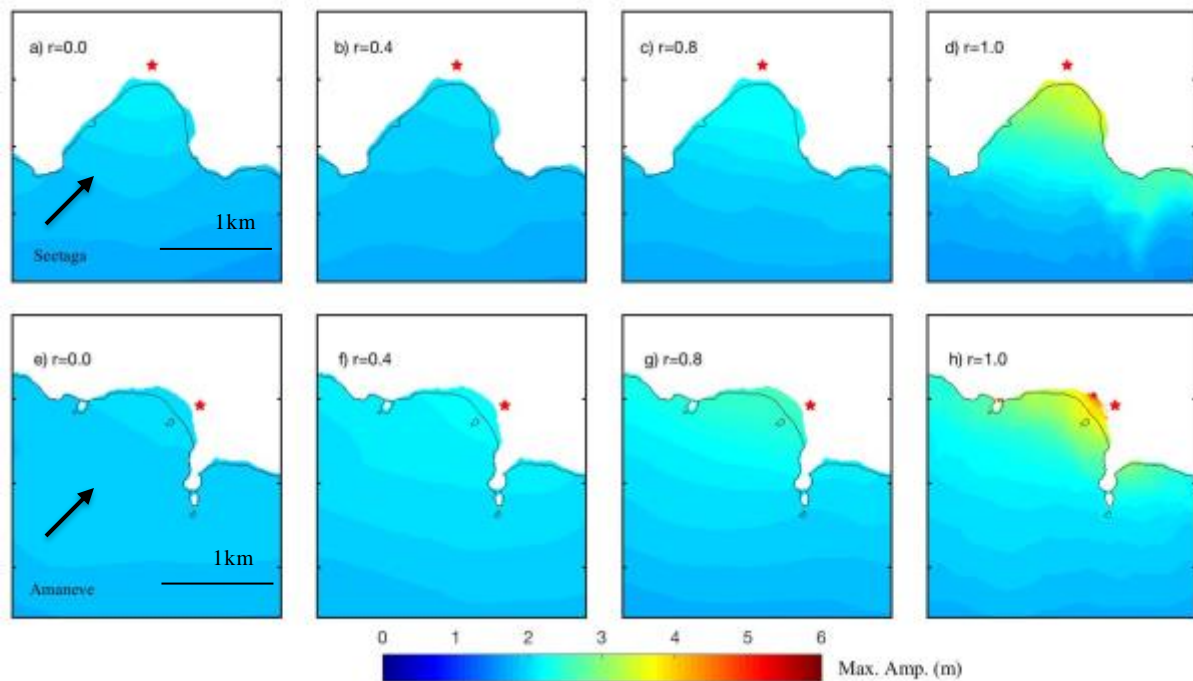
Figure 3.5. Simulated maximum wave amplitudes are shown for the bays near the villages of Seetaga (top panels) and Amaneve (bottom panel) for different bathymetry (r = 0.0, 0.4, 0.8 and 1.0). The pre-tsunami shoreline is shown as a thin black line. Colors inland of that line therefore show the degree of inundation. Village locations are shown as red stars. Black arrows indicate tsunami direction.

We also present simulated wave heights calculated at the same virtual tide gauges near Seetaga and Amaneve villages (Figure 3.6). In contrast to the results for varying n, changing the

54

bathymetry has a big impact on the wave dynamics recorded at the tide gauges. As the bathymetry is progressively removed ($r \to 0$), the first waves arrive 5 to 10 minutes earlier and the period of successive waves gets shorter, consistent with faster velocities in deeper water.
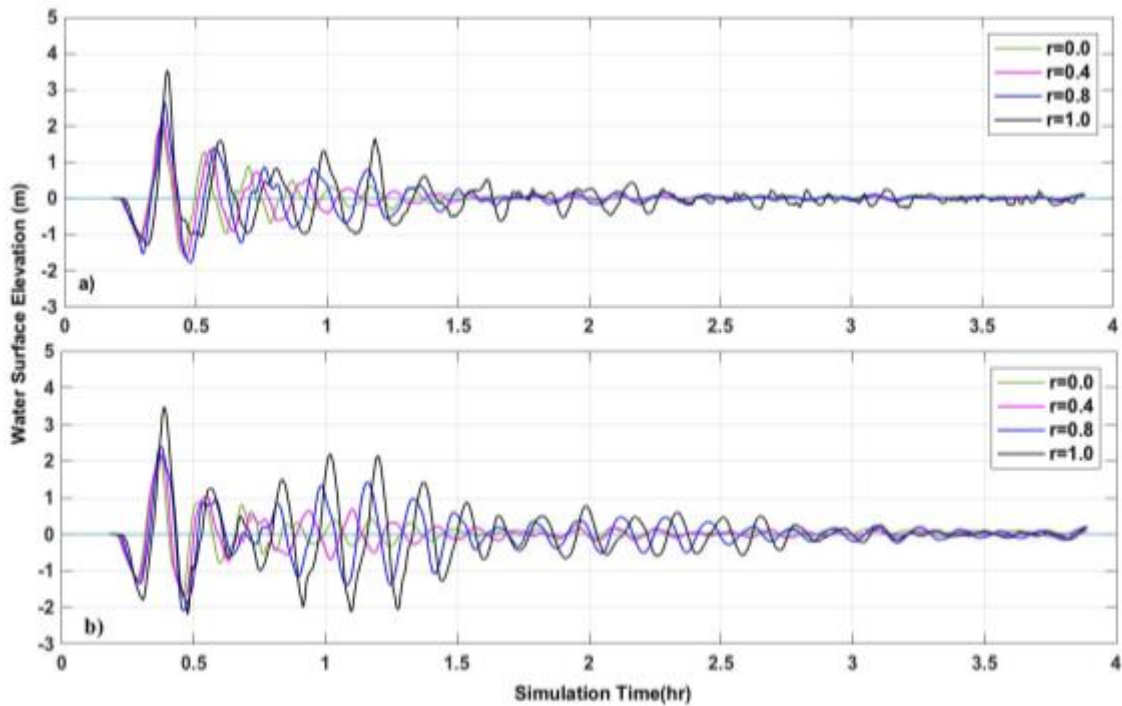
Figure 3.6. Comparison of water surface elevations at selected virtual tide gauges in the near-shore regions of villages of Seetaga and Amaneve. Refer to Figure 3.3 for location of gauges. Water surface elevations are given for varying r in the 4 h after the fault rupture at $t = 0$ (17:48:10 UTC, on Sep 29th, 2009).

\   A notable feature of the simulations is that varying the bathymetry has a big impact on the wave resonance that was observed to be particularly prominent in Seetaga bay (Figure 3.5a). As the bathymetry is progressively removed ($r \to 0$) the increase in amplitude of waves 4 to 7 seen in Seetaga Bay, diminishes and eventually disappears.   Obviously then, the bathymetry is playing an

important role in the constructive interference of reflected and incident waves. As the bathymetry is progressively removed, the first waves arrive earlier and the period of successive waves gets longer, consistent with faster velocities in deeper water. The dataset synthesized in Table A1 and A2 are summaries of the model results.

In a related study, Roeber, et al., 2010 showed the shortening of wave period by comparing their model results with the reef distribution around the island. In locations of observed higher run-up (i.e. Poloa, Fagasa, Tula and Pago Pago, the reefs extend from 0 m to at least 100 m from the shore. The reefs capture the tsunami waves and their energy and form wave resonances around the Tutuila Island. Wave resonances formed inside the bay cause increase in wave run-up on the coast. "The reefs trap the tsunami energy and worsen the impact of short period waves" (Roeber, et al., 2010).

3.1   DISCUSSION

The impact of the 2009 Samoa tsunami dynamics on the coral reefs of Tutuila island has been the main focus of this study. We conducted numerical model simulations of tsunami run-up and inundation at the coastal zones for varying Manning roughness, n, and reef bathymetry. For 31 villages on Tutuila island there is an overall tendency that when n decreases in the model, the estimated run-up values increase. However, the results are mixed with regard to whether different values of n improve the simulated run up compared to observations: the model estimation of run-up is improved by changing n in the model at some villages and doesn't change significantly at others.

Manning roughness, n, was spatially uniform in the simulations. Although this is standard practice in most current tsunami models, arguably such an approximation is only valid at large scales, and cannot capture the real situation of a heterogeneous reef environment. An important frontier in tsunami modeling research is whether, in pursuit of more accurate predictions, models should incorporate spatially varying n, or whether the mathematical representation of the dissipation (Eqns. 1 and 2) must be reformulated.

When we remove reefs, the modelled run-up values on the coast decrease, consistent with Green's law. A notable feature of the simulations is that varying the bathymetry has a big impact on the wave resonance that was observed. The bathymetry is playing a significant role in the constructive interference of reflected and incident waves. Inundation was not strongly impacted by varying the bathymetry, which suggests it is determined more by the coastal geometry than the tsunami wave dynamics. Rather than focusing on individual structures, we focused on reef bathymetry broadly around the island and to some degree our results must depend on the proximity of the reefs to the shore. Broader reefs further from shore, for instance, might dissipate wave energy enough to reduce onshore run up. Given the degree of complexity we found in simulations, it would, for instance, be hazardous to conclude that reefs provide universal protection for their inshore coastlines.

Chapter 4. CONCLUDING REMARKS

This study is the first attempt to quantify the relation between corals, tsunami run-up and tsunami dynamics. The role of reefs in tsunami dynamics remains enigmatic. Our results add to a body of literature exploring the important question: What is the role of reefs on tsunami dynamics for an island setting? The second chapter concludes that non-linear shallow water models have a

tendency to underestimate run-up in regions of high or very high coral damage, and that run-up tends to be better estimated in locations where coral damage is low. No clear relationship has been observed between coral damage and tsunami dynamics with the existing coral damage data of 2009 Samoa Tsunami.

In Chapter 3, at the first set of our experiments, for 31 villages on Tutuila island, there is an overall tendency that when n decreases in the model, the estimated run-up values increase. However, the model estimation of run-up is improved by changing n in the model at some villages and doesn't change significantly at others. Variation of Manning's n does not change the accuracy of run-up.

In the second set of experiments, we removed reef bathymetry and found that run-up decreases with removing the reef bathymetry. Rather than focusing on individual structures, we focused on reef bathymetry broadly around the island and to some degree our results must depend on the proximity of the reefs to the shore. Broader reefs further from shore, for instance, might dissipate wave energy enough to reduce onshore run up. Given the degree of complexity we found in simulations, it would, for instance, be hazardous to conclude that reefs provide universal protection for their inshore coastlines. We also found that the geometry of the bays is a more important factor than the bathymetry on determining the limits on inundation.

To conclude, while the impact of coral reefs on the dynamics of tsunamis impinging on tropical islands is obviously complicated and depends on many factors, our results reinforce a focus on two key issues that call for further research: first, the representation of the turbulent dissipation in terms of the governing equations and their coefficients and second, detailed numerical experiments on all aspects of reef settings such as reef widths, reef types and coastal geometry on the scale of individual bays.

BIBLIOGRAPHY

Abadie, S., Grilli, S., & Glockner, S. (2006). A Coupled Numerical Model for Tsunami Generated by Subaerial and Submarine MAss Failures. *30th Intl. Conf. Coastal Eng.* (pp. 1420-1431). San Diego: In Proc. 30th Intl. Conf. Coastal Eng.

Annunziato, A., Franchello, G., Ulutas, E., & Groeve, T. (2012). The 29 September 2009 Samoa Tsunami. *Journal of Tsunami Society, International, 31*(1), 19-61.

Baba, T., Mleczko, R., Burbidge, D., & Cummins, P. (2008). The Effect of Great Barrier Reef on the Propagation of the 2007 Solomon Islands Tsunami Recorded in Northeastern Australia. *Pure and Applied Geophysics, 165*, 2003-2018.

Baird, A. H., Campbell, S. J., & Anggoro, A. W. (2005). Acehnese Reefs in the Wake of the Asian Tsunami. *Current Biology, 15*(21), 1926-1930.

Baptista, M. A., Miranda, P. M., & Victor, L. M. (1998). Constrains on the Source of the 1755 Lisbon Tsunami Inferred from Numerical Modeling of Historical Data., *25*, pp. 159-174.

Beaven, J., Wang, X., Holden, C., Wilson, K., Power, W., Prasetya, G., . . . Kautoke, R. (2010). Near-simultenous Great Earthquakes at Tongan Megathrust and Outer-rise in September 2009. *Nature, 466*, 959-966.

Berger, M. J., & LeVeque, R. J. (1998). Adaptive Mesh Refinement Using Wave-Propagation Algorithms for Hyperbolic Systems. *SIAM J. Numer. Anal.*, 2298-2316.

Bernard , E. N., & Milburn, H. B. (1985, March 20). Long−wave Observations Near the Galápagos Islands. *Journal of Geophysical Research, 90*, 3361-3366.

Bernard, E. N. (2001). Tsunami: Reduction of Impacts Through Three Key Actions (TROIKA). *In Proc. Int. Tsunami Symp. 2001* (pp. 247-262). Seattle: ITS 2001.

Birkeland, C., Craig, P., Fenner, F., Smith, L., & Kiene, W. E. (2007). Geologic Setting and Ecological Functioning of Coral Reefs in American Samoa. In B. Riegl, & R. E. Dodge, *Coral Reefs of the USA* (pp. 741-765). Springer.

Borrero, J., Ortiz, M., Titov, V. V., & Synolakis, C. E. (1997). Field Survey of Mexican Tsunami Produces New Data, Unusual Photos. *EOS, 78*(8).

Bourgeois, J. (2009). Geologic Effects and Records of Tsunamis. In E. Bernard , & A. Robinson, *The Sea Tsunamis* (pp. 55-91). Cambridge, USA: Harvard University Press.

Brainard, R., Asher, J., Gove, J., Helyer, J., Kenyon, J., Mancini, F., . . . Vetter, O. (2008). Coral Reef Ecosystem Monitoring Report for American Samoa, 2002-2006. *National Marine Fisheries Service*, 1019-1020.

Bricker, J. D., Gibson, S., Takagi, H., & Imamura, F. (2015). On the Need for Larger Manning's Roughness Coefficients in Depth-Integrated Tsunami Inundation Models. *Coastal Engineering Journal, 57*(2), 1-13.

Caminade, P., Dougles, C. D., Kanoglu, U., Koshimura, S., Hideo, M. H., Moore, A., . . . Takahashi, T. (2000). Vanuatu Earthquake and Tsunami Cause Much Damage, Few Casualties . *EOS, 81*, 641-647.

Cartwright, J. H., & Nakamura, H. (2008). Tsunami: A History of the Term and of Scientific Understanding of the Phenomenon in Japanese and Western Culture. *Notes and Records of The Royal Society, 62*, 151-166.

Chatenoux, B., & Peduzzi, P. (2007). Impacts from the 2004 Indian Ocean Tsunami: Analyzing the Potential Protecting Role of Environmental Features. *Natural Hazards, 40*, 289-304.

Chow, V. T. (1959). *Open-Channel Hydraulics* (Vol. 113). New York: McGraw-Hill Book Company.

Clark, K., Power, W., Nishimura, Y., Atelea, R., Vaiomo'unga, R., Pongi, A., & Fifita, M. (2011, July). Characteristics of the 29th September 2009 South Pacific Tsunami as Observed at Niuatoputapu Island, Tonga. *Earth-Sciece Reviews, 107*(1-2), 52-65.

Dilmen, D. D., Roe, G. H., & Titov, V. V. (2015). Evaluation of the Relationship Between Coral Damage and Tsunami Dynamics; Case Study: 2009 Samoa Tsunami. *Pure and Applied Geophysics, 172 (12)*, 3557-3572.

Dilmen, D. I. (2009). *GIS Based Tsunami Inundation Maps; Case Studies From Mediterranean .* Middle East Technical University, Civil Engineering. Ankara: Middle East Technical University.

Fernando, H. J., McCulley, J. L., Mendis, S. G., & Perera, K. (2005). Coral Poaching Worsens Tsunami Destruction in Sri Lanka. *Eos Trans., 86*(33), 301-304.

Fernando, H. J., Samarawickrama, S. P., Balasubramanian, S., Hettiarachchib, S. S., & Voropayeva, S. (2008). Effects of Porous Barriers Such as Coral Reefs on Coastal Wave Propagation. *Journal of Hydroenvironment Research, 1*(3-4), 187-194.

Filloux, J. H. (1982, January). Tsunami Recorded on the Open Ocean Floor. *Geophysical Research Letters, 9*, 25-28.

Fritz, H. M., Borrero, J. C., Synolakis, C. E., Okal, E. A., Weiss, R., Lynett, P. J., . . . Chan, C. (2011). Insights on the 2009 South Pacific Tsunami in Samoa and Tonga from Field Surveys and Numerical Simulations. *Earth Science Reviews, 107*, 66-75.

Fujima, K. (2006). Effect of a Submerged Bay-Mouth Breakwater on Tsunami Behavior Analyzed by 2D/3D Hybrid Model Simulation. *Natural Hazards, 39*, 179-193.

Gelfenbaum, G., Apotsos, A., Stevens, A. W., & Jaffe , B. (2011). Effects of Fringing Reefs on Tsunami Inundation: American Samoa. *107 (1-2)*, 12-22.

George, D. L., & LeVeque, R. J. (2006). Finite Volume Methods and Adaptive Refinement for Global Tsunami Propagation and Local Inundation. *Science of Tsunami Hazards, 24 (5)*, 319-328.

Gica, E., Spillane , M. C., Titov, V. V., Chamberline, C. D., & Newman, J. C. (2008). Development of the Forecast Propagation Database for NOAA's Short-term Inundation Forecast for Tsunamis (SIFT). *NOAA Technical Momerandum, 139*, 89.

Gonzales, F., LeVeque, R. J., Chamberlain, P., Hirai, B., Varkovitzky, J., & George, D. L. (2011). GeoClaw Results for the NTHMP Tsunami Benchmarking Problems. *Natural Tsunami Hazard Mitigation Program*, 436.

Goto, C., & Ogawa, Y. (1997). *Numerical Method of Tsunami Simulation With the Leap-Frog Scheme.* Intergovernmental Oceanographic Commission, TIME Project, IUGG/IOC. Paris: UNESCO.

Green, G. (1837). On the Motion of Waves in a Variable Canal of Small Depth and Width. *Trans. Cambridge Philos. Soc., 6*, 457-462.

Gusiakov, V. K., Khidasheli, D. G., Marchuk, A. G., & Kalashnikova, V. (2007). *Analysis of Tsunami Travel Time Maps for Damaging Historical Tsunamis in the World Ocean.* IOC/UNESCO, NTL/ICMMG SD RAS. Novosbrisk: UNESCO.

Gusiakov, V. V. (2007). Tsunami History: Recorded. In E. Bernard, *The Sea* (pp. 23-54). Cambridge: Harvard University Press.

Gutenberg, B., & Richter, C. F. (1936). Magnitude and Energy of Earthquakes. *Science, 83 (2147)*, 183-185.

Harbitz, C., Lovholt, F., & Glimsdal, S. (2007). Mark Groudine. *Offshore Technology Conference* (pp. 10-19). Texas: Offshore Technology Conference.

Hebert, H., Heinrich, P., Schindele, F., & Piatanesi, A. (2001). Far-Field Simulation of Tsunami Propagation in the Pacific Ocean: Impact on Marquesas Islands (French Polynesia). *Journal of Geophysical Research, 106*(C5), 9161-9177.

Houston, J. R., & Garcia, A. W. (1974). *Type 16 Flood Insurance Study: Tsunami Predictions for Pacific Coastal Communities.* U.S. Army Engineer Waterways Experiment Station Hydraulics Laboratory. Vicksburg, Mississippi: U.S. Army Engineer Waterways Experiment Station Hydraulics Laboratory.

Igarashi, Y., Kong, L., Yamamoto, M., & McCreery, C. S. (2011). Anatomy of Historical Tsunamis: Lessons Learned for Tsunami Warning. *Pure and Applied Geophysics, 168*(11), 2043-2063.

Imamura, F. (1996). Review of Tsunami Simulation With a Finite Difference Method. *Long-wave Run-up Models*, 25-42.

Imamura, F., Goto, K., & Ohkubo, S. (2008). A Numerical Model for the Transport of a Boulder by Tsunami. *Geophysical Research Letter, 113*(C1), 113.

Irish, J., Ewing, L., & Jones, C. (2012). Observations from the 2009 Samoa Tsunami: Damage Potential in Coastal Communities. *Waterway, Port, Coastal, Ocean Eng, 138*(2), 131-141.

Jaffe, B. E., Gelfenbaum, G., Buckley, M. L., Watt, S., Apotsos, A., Stevens, A. W., & Richmond, B. M. (2010). The limit of inundation of the September 29, 2009, Tsunami on Tutuila, American Samoa. *U.S. Geological Survey Open File Report*(2010-1018), 27-37.

Jenks, G. F. (1967). The Data Model Concept in Statistical Mapping. *International Yearbook of Cartography, 7*, 186-190.

Kanamori, H. (1972). Mechanism of Tsunami Earthquakes. *Phys. Earth Planet. Interiors, 6*(5), 346-359.

Kirby, J., Wei, G., Chen, Q., Kennedy, A., & Dalrympl, A. (1998). *FUNWAVE 1.0,Fully Nonlinear Boussinesq Wave Model Documentation and Users Manual,Tech. Rep. Research Report No. CACR-98-06.* Center for Applied Coastal Research, University of Delaware, Delaware.

Kraines, S. B., Yanagi, T., Isobe, M., & Komiyama, H. (1998). Wind-wave Driven Circulation on the Coral Reef at Bora Bay, Miyako Island. *Coral reefs, 17*, 133-143.

Kunkel, M., Hallberg, R. W., & Oppenheimer, M. (2006). Coral Reefs Reduce Tsunami Impact in Model Simulations. *Geophysical Research Letters, 33 (23)*, 123612-123615.

Lautenbacher Jr., C. (2005). Tsunami Warning Centers. *National Academy of Engineering, 35*(2), 22-25.

Lay, T., Ammon, C. J., Kanamori, H., Rivera, L., Koper, K. D., & Hutko, A. R. (2010). The 2009 Samoa-Tonga Great Earthquake Triggered Doublet. *Nature, 466*(7309), 964-968.

Leschka, S., Kongko, W., & Larsen, O. (2009a). On the Influence of Nearshore Bathymetry Data Quality on Tsunami Run-up Modeling, Part1: Bathymetry. In X. H. Soon Keat Tan (Ed.), *5th International Conference on Asian and Pacific Coasts. 1*, pp. 151-156. Singapore: APAC.

Levin, B. W., & Mikhail, A. (2016). *Physics of Tsunamis.* Dordrecht, London: Springer International Publishing.

Lim, E., Taylor, L. A., Eakins, B. W., Carignan, K. S., Grothe, P. R., Caldwell, R. J., & Friday, D. Z. (2010). Digital Elevation Models of Pagopago, American Samoa: Procedures, Data Sources and Analysis. *NOAA Technical Momenrandum*, 26.

Liu, P. L., Wang, X., & Salisbury, A. J. (2009). Tsunami Hazard and Early Warning System in South China Sea. *Journal of Asian Earth Sciences, 36*(1), 2-12.

Liu, P. L., Woo, F., & Cho, Y. S. (1998). *Computer Programs for Tsunami Propagation and Inundation.* Cornell University. New York: Cornell University.

Lynett, P., & Lui, P. (2011). Numerical Simulation of Complex Tsunami Behavior. *Comput. Sci. Eng. , 13*(50), 50-57.

McDougall, I. (1985). Age and Evolution of the Volcanoes of Tutuila, American Samoa. *Pacific Science, 39*(4), 311-320.

Miller, G. R. (1972). Relative Spectra of Tsunamis. *Hawaii Inst. of Geophys., 72*(8), 7-10.

Mofjeld, H. (2009). Tsunami Measurements. In E. Bernard, & A. R. Robinson (Eds.), *The Sea, Tsunamis* (Vol. 15, pp. 201-235). Cambridge, USA: Harvard University Press.

Mori, N., Takahashi, T., Yasuda, T., & Yanagisawa, H. (2011). Survey of 2011 Tohoku Earthquake Tsunami Inundation and Run-up. *Geophysical Research letters, 38*, 1-10.

Murao, O. (2014). Recovery After Sanriku Tsunamis in 1896 and 1933, and Transition of Housing Location Before the 2011 Great East Japan Earthquake and Tsunami. In O. Murao, R. Shaw, & T. Izumi (Eds.), *Tohoku Recovery* (pp. 93-105). Tohoku, Japan: Springer.

NGDC/NOAA. (2015, May 1). *NGDC NOAA Natural Hazards*. (NOAA, Producer) Retrieved from https://www.ngdc.noaa.gov/hazard/

NGDC/WDS, N. G. (2015, June 1). *National Geophysical Data Center / World Data Service (NGDC/WDS)*. Retrieved from http://www.ngdc.noaa.gov/docucomp/page?xml=NOAA/NESDIS/NGDC/MGG/Hazards/iso/xml/G02151.xml&view=getDataView&header=none

NTHMP, N. T. (n.d.). Proceedings and Results of the 2011 NTHMP Model Benchmarking Workshop. *Proceedings and Results of the 2011 NTHMP Model Benchmarking Workshop. 436.* Boulder: US Department of Commerce NOAA/NTHMP.

Nunes, V., & Pawlak, G. (2008). Observations of Bed Roughness of a Coral Reef. *Journal of Coastal Research, 24*(2B), 39-50.

Okada, Y. (1985). Surface Deformation Due to Shear and Tensile Faults in a Half-Space. *Bull.Seism. Soc. Am., 75*, 1135-1154.

Okal, E. (2011). Tsunamigenic Earthquakes: Past and Present Milestones. *Pure and Applied Geophysics, 168*, 969-995.

Okal, E., Fritz, H., Synolakis, C. E., Borrero, J. C., Weiss, R., Patrick, L. J., . . . Chan, I. (2010). Field Survey of the Samoa Tsunami of 29 September 2009. *Seismological Reserch Letters, 81*(4), 577-591.

Okal, E., Synolakis, C. E., Uslu, B., Kalligeris, N., & Voukouvalas, E. (2009). The 1956 Earthquake and Tsunami in Amorgos, Greece. *Geophysical Journal international, 178*(3), 1533-1554.

Oskin, B. (2015, May 7). *Livescience*. Retrieved 7 1, 2016, from http://www.livescience.com/39110-japan-2011-earthquake-tsunami-facts.html

Paice, E. (2008). *Wrath of God: The Great Lisbon Earthquake of 1755*. London: Quercus.

Percival, D. B., Denbo, D. W., Eble, M., Edison, G., Motfjeld, H., & Spillane, M. C. (2011). Extraction of Tsunami Source Coefficients Via Inversion of DART Buoy Data. *Natural Hazards, 58*(1), 567-590.

Plafker, G. (1997). Catastrophic Tsunami Generated by Submarine Slides and Backarc Thrusting During the 1992 Earthquake on Eastern Flores 1., Indonesia. *Geol. Soc. Am. Cordill. Sect., 29*, 57-67.

Rabinovich, A. B. (1997). Spectral Analysis of Tsunami Waves: Seperation of Source and Topography Effects. *Journal of Geophysical Research, 102*(C6), 12663-12676.

Roeber, V., Yamazaki, Y., & Cheung, K. F. (2010). Resonance and impact of the 2009 Samoa Tsunami Around Tutuila, American Samoa. *Geophysical Research Letters, 37*(21), 21604.

Satake, K. (1994). Mechanism of the 1992 Nicaragua Tsunami Earthquake. *Geophysical Research Letters, 21*(4), 2519-2522.

Schidmore , E. (1896, 9 1). *National Geographic Magazine*. Retrieved from http://ngm.nationalgeographic.com/1896/09/japan-tsunami/scidmore-text

Shuto, N., & Fujima, K. (2009). A Short History of Tsunami Research and Countermeasures in Japan. *Proceedings of the Japan Academy. Series B, 85*(5), 267-275.

Sokolowski. (1990). *The Alaska Warning Center*. NOAA Technical Memorandum NWS AR-38. Alaska: National Weather Service.

Stokes, G. G. (1845). On the Theories of the Internal Friction of Fluids in Motion and of the Equilibrium and Motion of Elastic Solids. *Cambridge Philosophical Transactions, 8*(3), 287-305.

Sutherland, J., & O'Donoghue, T. (1998a). Wave Phase Shift at Coastal Structures. *Journal of Waterway, Port, Coastal and Ocean Engineering, 124*, 90-98.

Synolakis, C. E., & Okal, E. A. (2005). 1992-2002 Perspective on a Decade of Post Tsunami Surveys. *Advances in Natural and Technological Hazards Research, 23*, 1-29.

Synolakis, C. E., Bernard, E. N., Titov, V. V., Kanoglu, U., & Gonzales, F. I. (2008). Validation and Verification of Tsunami Numerical Models. *Pure and Applied Geophysics, 165*(11), 2197-2228.

Synolakis, C., & Kanoglu, U. (2009). Tsunami Modeling: Development of Benchmarked Models. In P. Lynette (Ed.), *Nonlinear Wave Dynamics. 1*, pp. 127-145. Novosibirsik: World Scientific, Singapore.

Tang, L., Titov, V. V., & Chamberline, C. D. (2009). Development, Testing and Applications of Site-specific Tsunami Inundation Models for Real-time Forecasting. *Journal of Geophysical Research, 114*(C12), 114-124.

Tang, L., Titov, V. V., Bernard, E., Wei, Y., Chamberline, C., Newman, J. C., . . . Spillane, M. (2012). Direct Energy Estimation of the 2011 Japan Tsunami Using Deep-Ocean Pressure Measurements. *Journal of Geophysics Research Letters, 117*(C8), 1-28.

Tappin, D. R., Watts, P., & Grilli, S. T. (2008). The Papua New Guinea Tsunami of 17 July 1998: Anatomy of a Catastrophic Event. *Natural Hazards Earth Syst. Sci., 8*(2), 243-266.

Terry, J. P., Kostaschuk, R. A., & Garimella, S. (2005). Sediment Deposition Rate in the Falefa River Basin, Upolu Island, Samoa. *Journal of Environmental Radioactivity, 86*(1), 45-63.

Thompson, R., Fine, I., Rabinovich, A., Muhaly, S., Davis, E., Heesemann, M., & Krassovski, M. (2011). Observation of the 2009 Samoa Tsunami by the NEPTUNE-Canada Cabled Observatory: Test Data for an Operational Regional Tsunami Forecast Model. *Geophysical Research Letters, 38*(11), L11701-L11708.

Tinti, S., & Tonini, R. (2013). Thr UBO-TSUFD Tsunami Inundation Model: Validation and Application to a Tsunami Case Study Focused on the City of Catania, Italy. *Natural Hazard and Earth System Sciences, 13*(7), 1795-1816.

Titov, V. V. (1997). Numerical Modeling of Long Wave Run-up. *University of Southern California, 58*(05), 2613-2628.

Titov, V. V. (2009). Tsunami Forecasting. In A. N. Bernard, A. R. Robinson, A. N. Bernard, & A. R. Robinson (Eds.), *The Sea, Volume 15: Tsunamis* (Vol. 15, pp. 371-400). Cambridge, MA, USA: Harvard University Press.

Titov, V. V., & Gonzales, F. I. (1997). Implementation and Testing of the Method of Splitting Tsunami (MOST) Model. *NOAA Technical Memorandum ERL PMEL, 11*, 30.

Titov, V. V., & Synolakis, C. E. (1998). Numerical Modeling of Tidal Wave Run-up. *Journal of Waterway, Port, Coastal and Ocean Engineering, 124*, 157-171.

Titov, V. V., Gonzales, F. I., Bernard, E. N., Eble, M. C., Motfjeld, H. O., Newman, J. C., & Venturato, A. J. (2003). Real-time Tsunami Forecasting: Challenges and Solutions. *Natural Hazards, 35*, 35-41.

Titov, V. V., Gonzales, F. I., Motfjeld, H. O., & Venturato, A. J. (2003). *NOAA TIME Seattle Tsunami Mapping Project: Procedures, Data sources, and Products.* Seattle: NOAA.

USGS. (2005, 1 1). *USGS.* Retrieved from http://earthquake.usgs.gov: http://earthquake.usgs.gov/earthquakes/eqinthenews/2004/us2004slav/us2004slav.php

Uslu, B., Eble, M., & Wright, L. (2013). A Tsunami Forecast Model for PagoPago Harbor, American Samoa. *NOAA Technical Memorandum, 19*, 1.

Wei, Y., Bernard, E., Tang, E., Weiss, L., Titov, V., Weiss, R., . . . Kanoglu, U. (2008). Real-Time Experimental Forecast of the Peruvian Tsunami of August 2007 for U.S. Coastlines. *Geophysical Research Letters, 35*(4), 1-7.

Whitmore, P. (2009). Tsunami Warning Systems. In E. Bernard, A. R. Robinson, & E. B. Robinson (Ed.), *The Sea* (Vol. 15, pp. 14-28). Cambridge, USA: Harvard University Press.

Yalciner, A. C., Zaytsev, A., Aytore, B., Insel, I., Heidarzadeh, M., Kian, R., & Imamura, F. (2014). A Possible Submarine Landslide and Associated Tsunami at the Northwest Nile Delta, Mediterranean Sea. *Oceanography, 27*(2), 68-75.

Zahibo, N., Pelinovsky, E., Yalciner, A. C., Kurkin, A., Koselkov, A., & Zaitsev, A. (2003). The 1867 Virgin Island Tsunami. *Natural Hazards and Earth System Sciences, 3*, 367-376.

Zahibo, N., Pelinovsky, E., Yalciner, A., Zaytsev, A., Talipova, T., Nikolkina, I., & Chernov, A. (2011). Trans-Atlantic propagation of 1755 tsunami and its effects on the French West Indies. *Open Oceanography Journal, 8*(5), 30-41.

Zhou, H., Wei, Y., & Titov, V. V. (2012). Dispersive Modeling of the 2009 Samoa Tsunami. *Geophysical Research Letters, 39*(16), 603-610.

APPENDIX A

We construct scatterplots by averaging the MOST output for maximum amplitude, current, flux, and stress along each survey track associated with a village (Figure 2.1), and plotting against the corresponding observed coral-damage numbers. The correlations for each scatter plot are given in the caption of Figure A1. None are statistically significant.
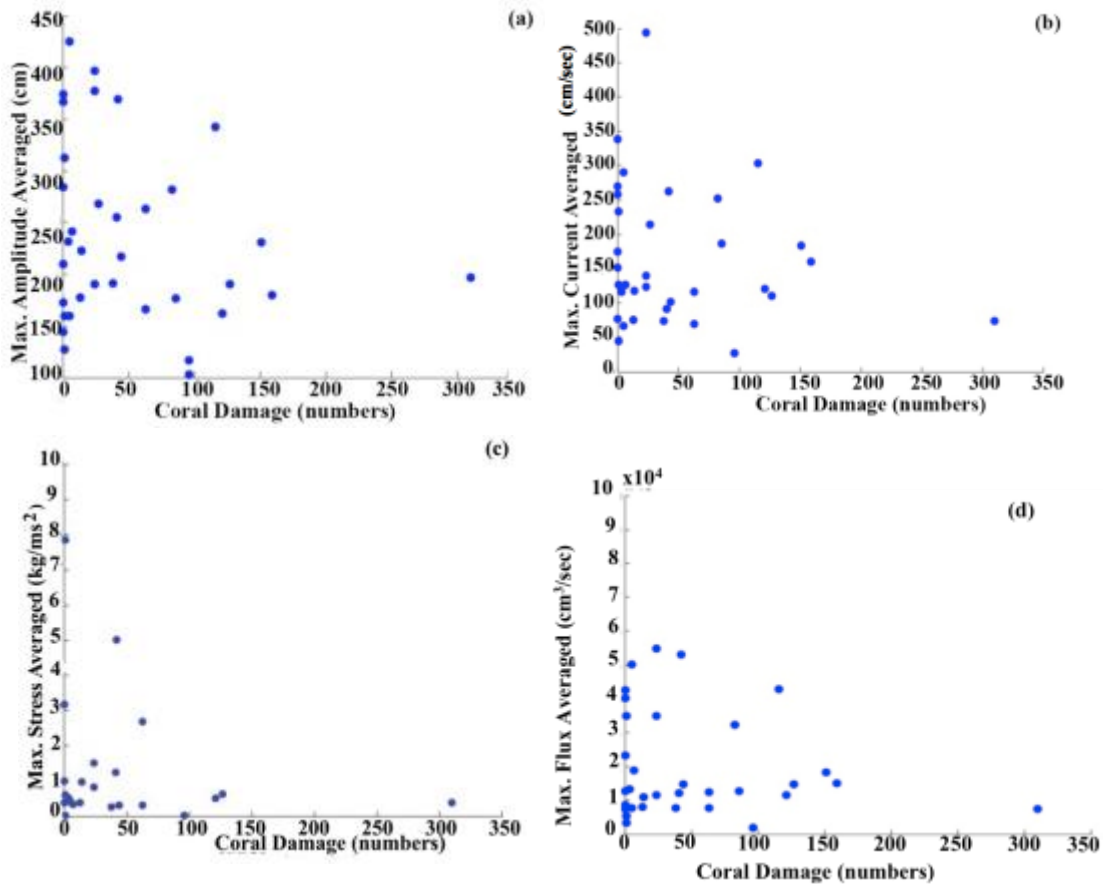
Figure A-1. Scatter plots of coral damage (on the *x*-axis) vs. (a) maximum amplitude; (b) maximum current; (c) maximum flux; and (d) maximum stress along coral damage track-lines. The dynamical fields are averaged over each track-lines associated with each village (Figure 2.1), to evaluate any relationship between coral damage and dynamical fields.

APPENDIX B

These tables present MOST model output for maximum amplitude along selected villages (Figure 2.1 for locations of the villages). There is a tendency that run-up increases with decreasing Manning and the model better estimates run-up. (Table B1). There is also a tendency that run-up decreases with removing reefs (Table B2).

Table B1. Model, simulated run-up for different Manning's roughness, n, values at 31 villages around Tutuila.

Villages	Field Run-up(m)	Run-up, n=0.08	Run-up, n=0.06	Run-up, n=0.04	Run-up, n=0.03	Run-up, n=0.02	Run-up, n=0.015
LAUILI	3.36	1.35	1.58	1.78	1.80	2.12	2.35
AMALAU	2.5	1.46	1.49	1.52	2.12	1.55	1.72
AFONO1	2.18	1.92	1.98	2.06	3.00	2.20	2.45
AFONO2	3.8	2.04	2.11	2.21	3.50	2.41	2.68
AVAIO	3.7	2.81	2.95	3.12	3.15	3.59	3.98
MASEFAU	4	3.32	3.30	3.27	4.20	3.37	3.74
AMAUA	2.91	3.05	3.23	3.43	3.20	3.81	4.23
FAGAITUA	3.5	3.60	4.26	5.02	4.75	5.31	5.90
MASAUSI	2.79	2.46	2.48	2.50	3.15	2.56	2.84
SAILELE	2.95	1.99	2.01	2.01	2.25	2.00	2.23
AOA	2.23	1.36	1.60	1.82	2.20	2.05	2.28
AMOULI	3.15	2.76	3.18	3.53	3.20	4.18	4.64
ONENOA	3.6	2.20	2.21	2.23	2.50	2.24	2.48
AUASI	3.79	2.57	3.06	3.47	3.08	3.73	4.14
TULA	7	3.11	3.44	3.66	3.80	3.89	4.32
AUNUU	2.15	1.54	1.71	1.85	2.14	2.03	2.25
POLOA	13.23	6.10	6.49	7.03	7.30	7.62	10.74
AMANAVE	7.74	4.69	4.85	4.93	5.25	6.32	5.79
FAGAILII	6	4.77	4.78	4.84	4.90	5.33	7.90
FAILOLO	6.54	2.87	2.79	2.69	2.70	3.29	3.14
AGUGULU	6.12	1.93	2.11	2.35	2.50	2.23	2.43
UTUMEA	4.51	3.05	3.15	3.76	4.00	4.52	5.68
SEETAGA	5.69	4.98	5.09	5.50	5.57	6.29	5.19
FAGAMALO	6.39	2.88	3.22	3.37	3.30	3.30	15.00
NUA	4.09	3.61	3.86	4.15	4.20	3.85	3.86
AFAO	5.89	3.46	3.83	4.10	4.20	3.98	4.74
ASILII	6.81	5.05	5.30	5.66	6.00	6.94	5.74
AMALUIA	5.39	5.14	5.26	5.26	5.20	5.60	6.21
LEONE	2.8	1.26	1.89	2.58	3.00	2.66	2.01
FAGATELE	4.92	3.12	3.21	3.28	3.30	3.33	3.33

Table B2. Model, simulated run-up for different *r* values representing varying bathymetry at 31 villages around Tutuila.

Villages	Field Run-up (m)	Run-up, r=1	Run-up, r=0.8	Run-up, r=0.6	Run-up, r=0.4	Run-up, r=0.2	Run-up, r=0.0
LAUILI	3.36	1.8	1.13	1.05	0.98	0.94	0.89
AMALAU	2.5	2.12	2.05	1.89	1.76	1.65	1.54
AFONO2	2.18	3	2.34	2.30	2.33	2.24	2.17
AFONO1	3.8	3.5	2.70	2.79	2.75	2.77	2.72
AVAIO	3.7	3.15	2.46	2.25	2.25	2.27	2.30
MASEFAU	4	4.2	2.80	2.49	2.58	2.61	2.70
AMAUA	2.91	3.2	1.93	1.86	1.79	1.75	1.67
FAGAITUA	3.5	4.75	3.14	2.78	2.86	2.88	2.95
MASAUSI	2.79	3.15	2.15	2.10	1.99	1.95	1.98
SAILELE	2.95	2.25	1.55	1.63	1.47	1.49	1.43
AOA	2.23	2.2	1.90	1.76	1.72	1.69	1.63
AMOULI	3.15	3.2	3.67	2.87	2.93	2.87	2.80
ONENOA	3.6	2.5	1.69	1.41	1.42	1.40	1.33
AUASI	3.79	3.08	2.24	2.16	2.02	2.02	1.88
TULA	7	3.8	2.38	2.22	2.07	2.07	1.98
AUNUU	2.15	2.14	2.07	1.90	1.78	1.78	1.67
POLOA	13.23	7.3	5.32	5.12	4.79	4.46	4.14
AMANAVE	7.74	5.25	3.29	3.06	2.85	2.73	2.59
FAGAILII	6	4.9	4.75	4.36	4.08	3.82	3.56
FAILOLO	6.54	2.7	2.11	2.07	2.10	2.02	1.95
AGUGULU	6.12	2.5	1.93	1.99	1.96	1.98	1.94
UTUMEA	4.51	4	3.12	2.86	2.86	2.88	2.92
SEETAGA	5.69	5.57	3.71	3.30	3.43	3.46	3.59
FAGAMALO	6.39	3.3	1.99	1.92	1.84	1.81	1.72
NUA	4.09	4.2	2.78	2.46	2.53	2.54	2.17
AFAO	5.89	4.2	2.87	2.80	2.65	2.60	2.64
ASILII	6.81	6	4.14	4.34	3.91	3.96	3.83
AMALUIA	5.39	5.2	4.50	4.15	4.06	4.01	3.86
LEONE	2.8	3	3.44	2.69	2.75	2.69	2.62
FAGATELE	4.92	3.3	2.23	1.85	1.88	1.85	1.75

VITA

Author of this research is born and raised in Turkey. She came to US to study her PhD. At University of Washington with the privilege of getting fellowship from Joint Institute for the Study of Atmosphere and Ocean, University of Washington. She gained interest into tsunami science starting from her senior level in Middle East Technical University, Ankara, Turkey. She published two peer-reviewed papers and coauthored three papers during her education. She takes motivation of working on tsunami science by thinking that she can save a person's life from tsunamis. She can speak English, Turkish and German fluently. She likes to ski, swim, and travel.

Education:

PhD: Department of Earth and Space Sciences, 2009-2016, University of Washington, Seattle, WA, USA;

B. Sc. & M.S.: Civil Engineering (Hydromechanics & Ocean), 2002-2009, Middle East Technical University-METU, Ankara, Turkey;

Publications:

1. Dilmen, D. I. (2009). *GIS Based Tsunami Inundation Maps; Case Studies From Mediterranean.* Masters Thesis, Middle East Technical University, Civil Engineering. Ankara,Turkey.

2. Dilmen D I., Kemec S., Yalciner A. C., Duzgun S., Zaytsev A., (2014), Development of Tsunami Inundation Map in Detecting Tsunami Risk in Gulf of Fethiye, Turkey, Pure Appl. Geophys. 2014 Springer Basel.

3. Dilmen D I., Titov V.V., Roe, G.H. (2015), Evaluation of the Relationship Between Coral Damage and Tsunami Dynamics; Case Study: 2009 Samoa Tsunami, Pure Appl. Geophys. 2015 Springer Basel.

4. **Kemec S., Duzgun S., Zlatanova S., Dilmen D. I., Yalciner A. C., (2010)**, Selecting 3D Urban Visualisation Models for Disaster Management: Fethiye Tsunami Inundation Case, Proceedings of TIEMS 2009 Annual Conference, Istanbul.

5. **Pelinovsky, E., Zahibo N., Yalciner A., Zaitsev A., Talipova T., Chernov A., Insel I., Dilmen D., Ozer C., Nikokina I., (2009)**, 1755 Tsunami Propagation in Atlantics and its Effects on the French West Indies, Geophysical Research Abstracts, Vol. 11, EGU2009-502, 2009 EGU General Assembly.

6. Yalciner A. Y., Gulkan P., Dilmen D. I., Aytore B., Ayca A., Insel I., Zaytsev A., (2014), Evaluation of Tsunami Scenarious for Western Peoponnese, Greece, Bollettino do Geofisica Teorica ed Applicata.

Related Work Experience:

1. Research (GSRA) and Teaching Assistant (TA) at University of Washington, Seattle

2. Project Engineer at European Union Funded Research Projects SEEHELLARC and TRANSFER, METU, Turkey